공학박사학위논문

Electrochemical investigation on structural components of triethylene glycol-based levelers with bromide ions for bottom-up filling in microvia

마이크로비아에서 바닥 차오름을 위한

브로마이드 이온과 트라이에틸렌글라이콜을 기반한

평탄제의 구조적 요소들에 대한 전기화학적 연구

2021년 2월

서울대학교 대학원

화학생물공학부

이 명 현

Electrochemical investigation on structural components

of triethylene glycol-based levelers with bromide ions

for bottom-up filling in microvia

마이크로비아에서 바닥 차오름을 위한
브로마이드 이온과 트라이에틸렌글라이콜을 기반한
평탄제의 구조적 요소들에 대한 전기화학적 연구

지도교수 김 재 정

이 논문을 공학박사 학위논문으로 제출함
2020 년 12 월

서울대학교 대학원
화학생물공학부
이 명 현

이명현의 공학박사 학위논문을 인준함
2021 년   2 월

위 원 장   김 영 규   (인)

부위원장   김 재 정   (인)

위   원   이 규 태   (인)

위   원   김 수 길   (인)

위   원   김 명 준   (인)

Abstract

Copper (Cu) electrodeposition is a commonly utilized technology for the metallization in printed circuit boards and integrated circuits in the electronics industry. For the high responsibility of metallization, bottom−up filling is achieved by using various additives. Levelers play a role in bottom−up filling of microvia among the additives, which is necessary to develop for better filling performance. It is necessary to modify the structure of levelers for enhancing the inhibition effect, but studies on the inhibition behavior of leveler according to structures are still insufficient. In this study, the interaction between bromide ions and accelerator and modifying the structures, such as terminal functional groups and quaternary ammonium groups, on triethylene glycol (TEG)−based levelers are examined to improve the inhibition strength.

First study investigates the effect of bromide ions on the adsorption of polymeric suppressor and accelerator. Although bromide ions are used as the counter ions, they can be applied as the inorganic additive. Bromide ions indicate the inhibition effect and stabilize the inhibition layer of suppressor on the Cu surface. The competitive adsorption with the accelerator is dependent on the concentration of accelerator and bromide ions and the forced convections. In the range of concentration ratio (0.2 < [SPS]/[Br$^-$] < 0.7), microvias can form bottom−up filling by depositing Cu at the

corner of bottom in microvias and inhibiting the top surface of microvias. The conformal filling is achieved if the concentration ratio is out of that range.

Bromide ions are chosen as the counter ions in TEG−based levelers because of the inhibition effect produced by the interaction with additives. Levelers are necessary to modify the structure for compensating the insufficient inhibition because the displacement of I^- to Br^- reduces the inhibition effect of levelers. To enhance the inhibition property of levelers, TEG−based levelers varying the terminal functional groups (allyl, propyl, benzyl, and naphthylmethyl) are synthesized. Among the synthesized levelers, the leveler composed of naphthylmethyl groups indicates the strongest inhibition effect and no deactivation by accelerator. In microvia filling, filling ratio reaches 100% within 50 min and the top thickness of microvia is 15 μm by using three−additives containing the leveler. As a results, naphthylmethyl groups are advantageous for enhancing the inhibition strength of leveler.

In addition, quaternary ammonium groups can be related to the adsorption of levelers because of their positive charge. We also investigate the inhibition effect of levelers according to the number of quaternary ammonium groups. The leveler containing three−ammonium groups induces the strongest inhibition effect among the synthesized levelers in this study. And it shows that the interaction between the leveler

and accelerator make the synergistic inhibition by the competitive adsorption. In specific concentrations of additives, bottom−up filling is formed by using the leveler with three−ammonium groups, which also can be achieved by enhancing the current density from 15 to 30 mA/cm^2 in the accelerator and leveler composition. Astonishingly, the Cu deposition time is reduced from 60 to 30 min.

These studies can be helpful for analyzing and suggesting new levelers in the Cu electrodeposition industry.

Keywords: Microvia, Cu, electrodeposition, leveler, bromide ion, terminal functional groups, quaternary ammonium groups, bottom−up filling

Student number: 2015−21076

Content

List of Tables

List of Figures

CHAPTER I

Introduction

1.1. Cu interconnects in electronic devices

Newly developed semiconductor devices should include various copper (Cu) interconnects which carry current or transport charge. In 1960, aluminum (Al) or Al+silicon (Si)+Cu alloy as the beginning material applied to interconnecting lines.[1,2] However, Al interconnects induce higher resistivity and electron migration in the shrinking circuit dimensions.[3] Cu interconnects were firstly utilized in the integrated circuits (ICs) by IBM in 1997.[4] Cu interconnects present faster operating speed compared to Al interconnects because of lower resistivity (Cu: 1.67 $\mu\Omega\cdot$cm, Al: 2.66 $\mu\Omega\cdot$cm).[5] Damascene technology is introduced to fabricate Cu interconnects. Its process requires patterning of deposited dielectric material, formation of seed and barrier layer, Cu electrodeposition, and chemical mechanical planarization process. The semiconductor industry requires smaller feature size, lower power consumption, and higher circuit density for high performance devices. As a results, multi–layered interconnects are developed by repeating the fabrication of Cu interconnects and

introduced by logic device industries as shown in Fig. 1.1.[6] Microvia or through holes

(THs) have a role as the interconnection between conducting layers in printed circuit

boards (PCBs).[7–9] The packing substrates of IC chips in Fig. 1.2[10] and the motherboard

of electronic devices require a high density interconnection (HDI) to improve the

electrical connection and shrinkage effect. Therefore, interconnects can also be

fabricated by laser drilling process to shrink the size of features to be $50 \sim 125$ μm.[11] The

semiconductor device technology keep up the extreme scaling to enhance the chip

performance. However, International Roadmap for Devices and Systems (IRDS)

suggested that the limitation of scaling on chip would encounter by its scale.[12]

Accordingly, 3D packaging technology such as wire bonding and through–silicon vias

(TSVs) has been studied to overcome the scaling problem, as shown in Fig. 1.3.[13] Lower

energy consumption, better electrical performance and higher density resulted from the

shortest vertical interconnection of TSVs because the wire bonding has a space limitation

to the miniaturization of chip size.[14,15]
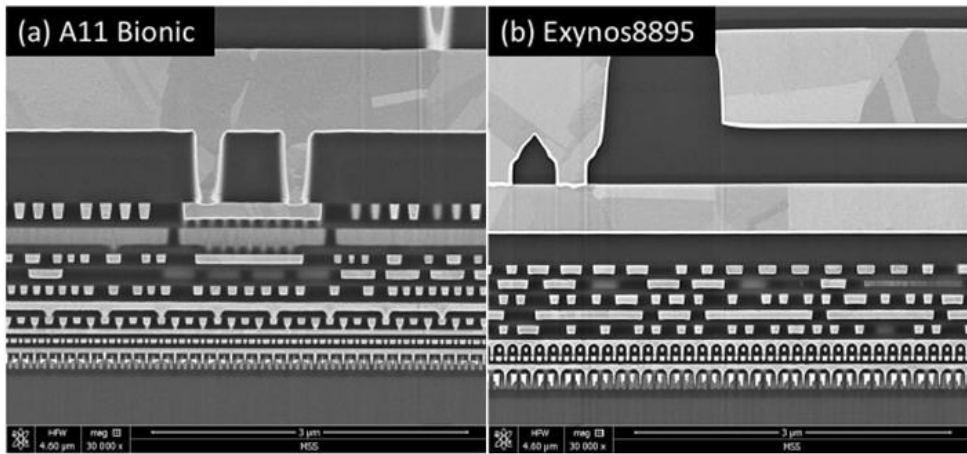
Figure 1.1. Cross–sectional images of (a) A11 Bionic and (b) Exynos8895 with 10 nm

node. (Ref. 6)
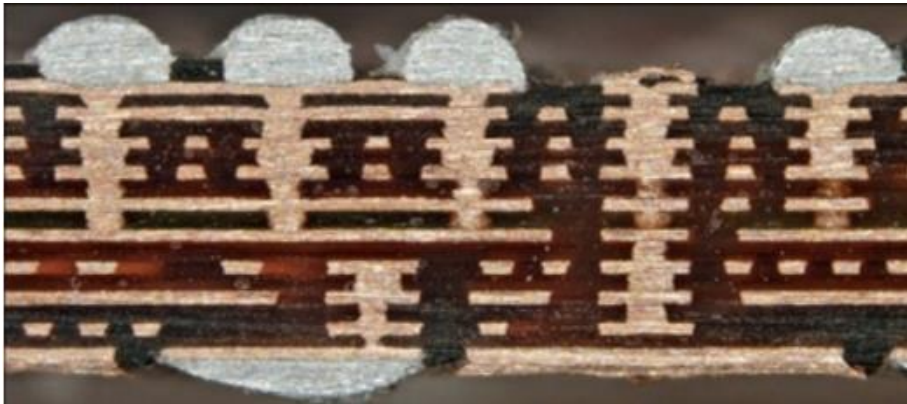
Figure 1.2. Microvias of Apple's 10–layer on iPhone 4 logic PCB board. (Ref. 10)
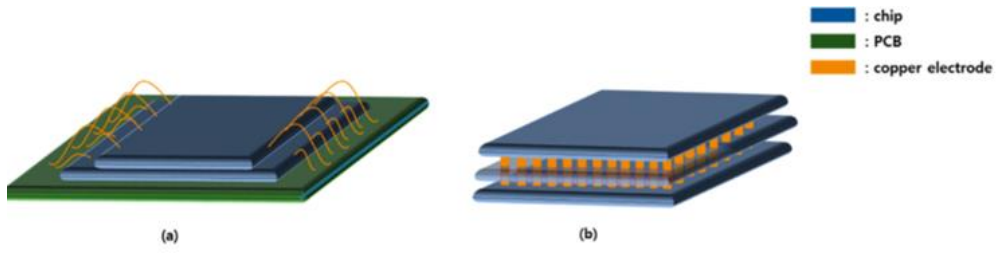
Figure 1.3. 3D packaging technologies by (a) wire bonding and (b) TSVs. (Ref. 13)

1.2. Filling of microvia by Cu electrodeposition

Cu electrodeposition is a process to reduce Cu ions in the electrolyte on the electrode by electrons, as shown in Fig. 1.4. Cu seed layers are required for making the conductive substrate as the working electrode in the electrochemical process. Cu ions reach the electrode surface through mass transfer. The reduction of Cu ions occurs by two charge transfer steps in Cu electrodeposition. The reaction from cupric ions (Cu^{2+}) to cuprous ions (Cu^+) determines the growth rate of Cu as the rate determining step. And then Cu is deposited by faster reduction of Cu^+ than the above reaction.[16] Cu oxidation reaction or dissolution is simultaneously observed at the counter electrode during the electrodeposition process. The electrolyte is commonly composed of Cu compound for providing Cu ions and supporting electrolyte that reduces the solution resistance.

Cu electrodeposition is a key technology for fabricating high conductive Cu interconnections for electronics, including semiconductor devices and PCBs. The interconnects, such as damascene interconnects with a width of hundreds or tens of nanometers,[17,18] TSVs with a diameter of 5 μm and a depth of 50 μm,[13,19–21] microvias,[22,23] and THs[24] are filled by Cu electrodeposition. The defects, such as the seams or voids, inside the features should be avoided to assure the reliability and better

electrical performance when the features are filled by Cu electrodeposition. As a results, filling profiles are classified into three structures as shown in Fig. 1.5. Subconformal deposition is the structure when the entrance of microvias is blocked by Cu deposited at the edge. Cu ions are preferentially consumed for the deposition near the entrance of microvias due to high current density at the edge. The mass flow of Cu ions is obstructed by the growth of Cu on the edge of entrance. As a results, voids are formed at the bottom of microvias. The same deposition rate on all surface of microvias results in conformal deposition with the seam. After the annealing process, the defects in subconformal or conformal deposition of microvias enlarge by the repetitive operation of devices.[25,26] Therefore, void–free filling is definitely required for the reliability and higher electrical performance. Superconformal deposition, or so–called superfilling and bottom–up filling, is caused by more rapid deposition rate at the bottom of microvia and trench, which induce bottom–up growth of Cu.[27–29] In order to achieve this bottom–up filling, the synergistic effect of additives is essential to Cu electrodeposition in microvia filling process.
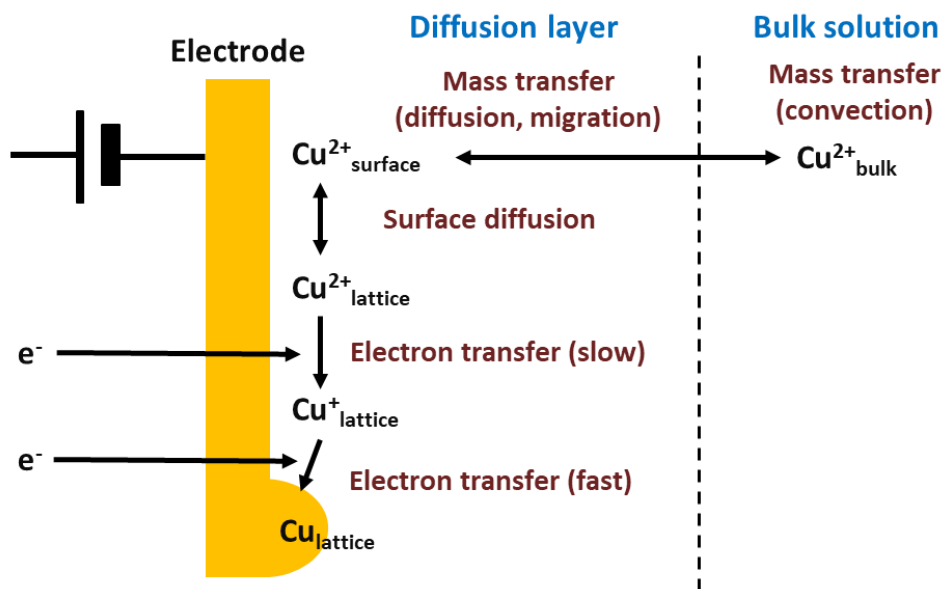
Figure 1.4. Schematic diagram of Cu electrodeposition in Cu electrolyte.
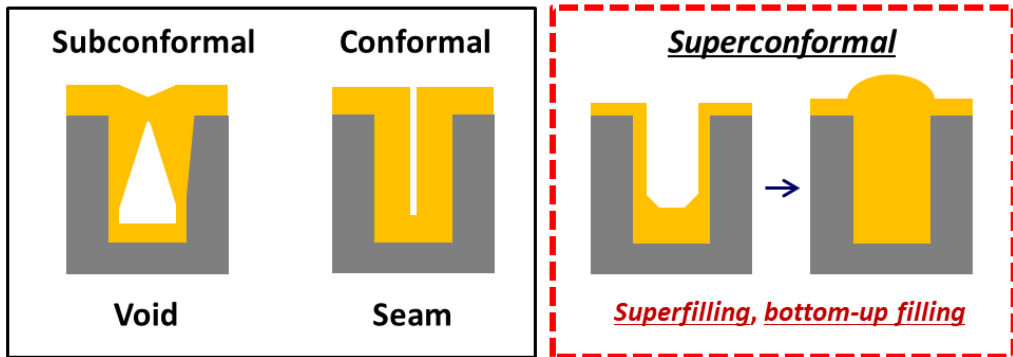
Figure 1.5. Deposition profiles of microvia filling by Cu electrodeposition. Subconformal, conformal, and superconformal (superfilling or bottom–up filling) deposition.

1.3. Additives for bottom–up filling

In general, organic additives applied in Cu electrodeposition induce bottom–up filling by affecting the deposition rate. The additives are categorized into two types on the basis of the effect on deposition rate: accelerator and suppressor which enhances and inhibits the deposition rate of Cu, respectively. The representative accelerators and suppressors used in Cu electrodeposition are enumerated in Fig. 1.6.
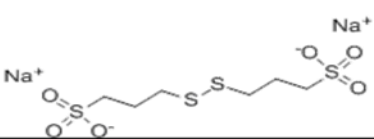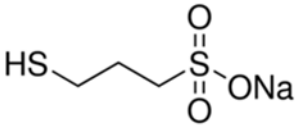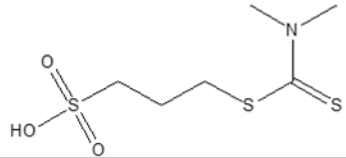
The accelerators are usually composed of 3–mercapto–1–propanesulfonic acid sodium salt (MPSA), bis(3–sulfopropyl) disulfide disodium salt (SPS), and 3–N, N–dimethylaminodithiocarbamoy–1–propanesulfonic acid (DPS).[8,30–33] Mercapto groups (–SH) and disulfide bond (–S–S–) contained in the accelerators make the acceleration by the following interconversion mechanism.[34,35] The generated Cu^+ by comproportionation reaction and intermediate of Cu reduction reduces SPS to thiolate$^-$ that is followed by the reformation of disulfide bond (SPS) accompanying the reduction of Cu^{2+} to Cu^+–thiolate$^-$. Cu–thiolate is reduced to Cu during the electrodeposition. For this reason, the consecutive reaction containing the interconversion between SPS and MPS induces the acceleration of Cu reduction.

The suppressors are typically polyether molecule such as polyethylene glycol (PEG),

polypropylene glycol (PPG), and their block copolymers (PEG–PPG and PPG–PEG–PPG), which are adsorbed on Cu surface to constitute inhibition layers and induce the over potential to inhibit Cu deposition.[36] Chloride ions (Cl^-) are complexed with the suppressor on the Cu surface that is covered by the form of PEG–Cu^+–Cl^- [37–39] or PEG–Cl^- [40–42]. The adsorbed inhibition layers directly control the approach of Cu^{2+} on the Cu surface, thereby decreasing the charge transfer rate of Cu deposition.

The interaction between the accelerator and the suppressor has a key role to explain bottom–up filling mechanism in Damascene process. The accelerator and the suppressor are both adsorbed on the Cu surface within a very short filling time, enabling the accumulation of accelerators by area reduction at the bottom corner of the features, which results in bottom–up Cu filling, as theoretically described in the curvature enhanced accelerator coverage (CEAC) model in Fig.1.7.[43–45] The filling process is completed within minutes owing to the small feature sizes.[29,46]

< Accelerator >

Chemical name	Molecular structure
Bis(sulfopropyl) disulfide disodium salt (SPS)	
3-Mercapto-1-propanesulfonic acid sodium salt (MPSA)	
3-N,N-dimethylamino dithiocarbamoyl-1-propanesulfonic acid (DPS)	

< Suppressor >
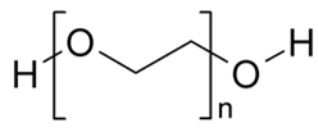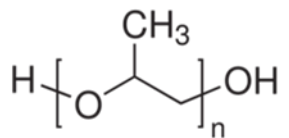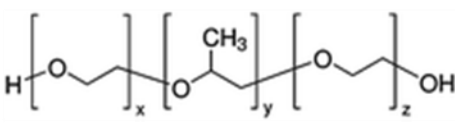
Chemical name	Molecular structure
Polyethylene glycol (PEG)	
Polypropylene glycol (PPG)	
Polyethyleneglycol-polypropyleneglycol block copolymer (PEG-PPG)	

Figure 1.6. Representative accelerator and suppressor for Cu electrodeposition.
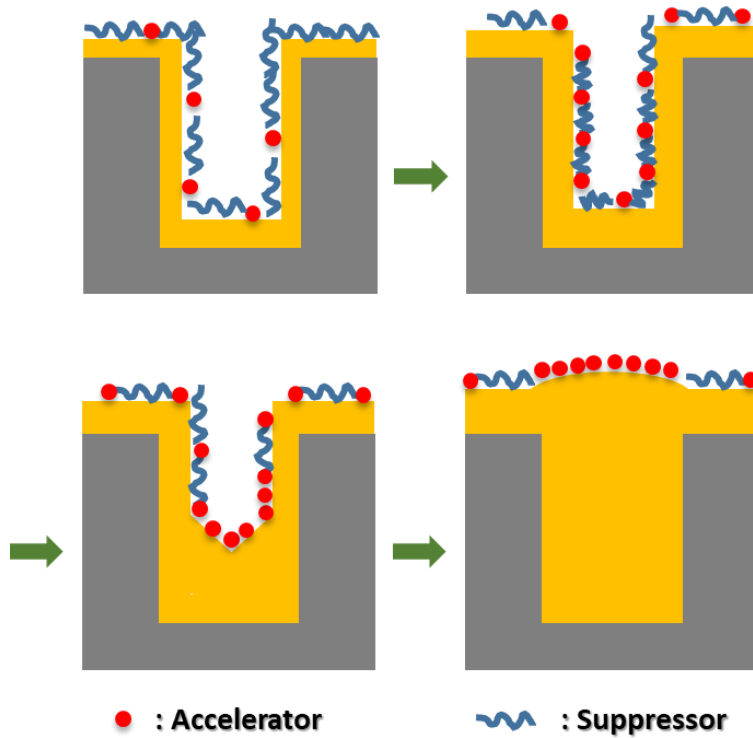
Figure 1.7. Schematic diagram of Cu bottom–up filling with CEAC model.

1.4. Leveler and its structural characteristic

   Micro–scale features including microvias, THs, and TSVs need a longer electrodeposition time to achieve the complete Cu filling because of their larger feature sizes.[47,48] In these cases, the accelerators could cover the entire Cu surface after displacing most of the co–adsorbed suppressors, whereby accelerator accumulation at the bottom of the features would be impossible. Therefore, the leveler is introduced into the combination of accelerator and polymeric suppressor.[48,49] The leveler also decreases the deposition rate of Cu and promotes the development of a homogeneous surface through convection–dependent adsorption (CDA) behavior.[50,51] The adsorption and inhibition functions of the leveler become more severe when the forced convection of the electrolyte becomes more vigorous. Generally, the electrolyte in the vicinity of the bottom of microvias is quiescent compared to that at the top of microvias, and thus CDA enhances the deposition rate at the bottom, as shown in Fig. 1.8.[50] If the leveling effect appears correctly, the bottom is deposited thicker as shown in Fig. 1.8 (a) while the plating process with the same thickness, as Fig. 1.8 (b), is performed without the leveling effect.

Leveler is important to achieve bottom–up filling of microvias based on CDA behavior as mentioned above. In early study, Janus Green B (JGB) is a widely used leveler that contain one quaternary ammonium cation group and Cl^-. Fig. 1.9 indicates the comparison of filling performance and potential profiles by JGB and benzotriazole (BTA).[48] JGB preferentially adsorbs on the protrusion of Cu to suppress the deposition rate of Cu because of the selective adsorption of the quaternary ammonium group.[52] The addition of JGB results in the mirror–like surface of Cu deposition. BTA shows the conformal filling because it could not form the inhibition difference like JGB. In Fig. 1.10, dye–type levelers having a similar filling performance to JGB are also studied, including Diazine Black, Alcian Blue, and Safranin T.[22,23,27,49] The quaternary ammonium groups of levelers are adsorbed on the protrusion of Cu surface and inhibit the reduction of Cu^{2+} during Cu electrodeposition. However, the addition of JGB into Cu electrolyte causes the instability of Cu plating solution.[24,52] The quaternary ammonium groups positively ionized in Cu electrolyte reach to Cu surface by electrostatic interaction and adsorb on Cu surface to inhibit the reduction of Cu. For the reason, these functional groups have been proved as the effective leveling agent.

Based on the results of JGB, the molecular structure of levelers containing quaternary ammonium groups has an influence on Cu electrodeposition. Many researchers have

developed new levelers to enhance the inhibition effect and filling performance. In particular, the inhibition effect of levelers can be varied by modifying the structure of levelers, such as the functional groups,[27,53–55] side chain length,[56–58] aromatic rings,[59,60] and counter ions.[28,61,62] Studying the structure–property relationship of additives could assist in understanding the inhibition mechanism of levelers for achieving bottom–up filling and designing the new levelers.
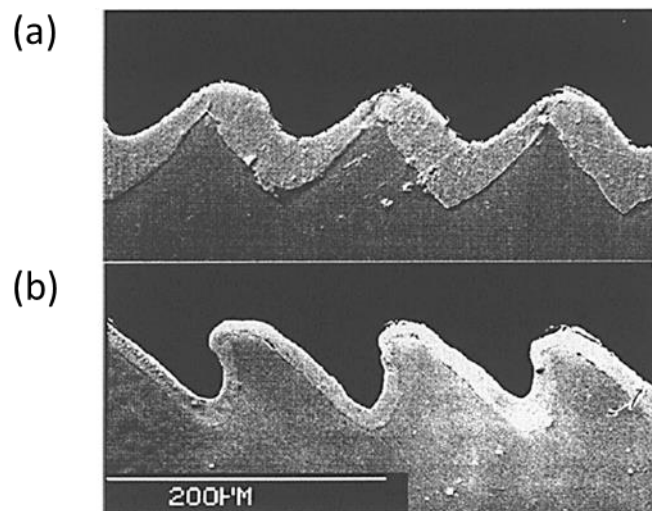
Figure 1.8. Cross–sectional SEM images showing the leveling performance of Cu

electrolyte with SPS and JGB. (Ref. 50)
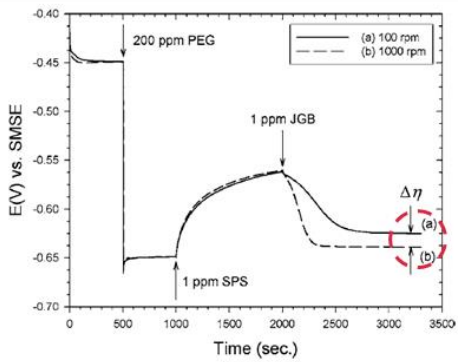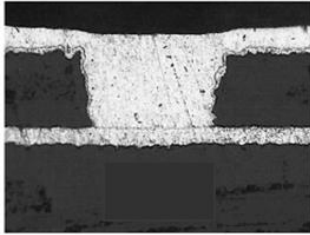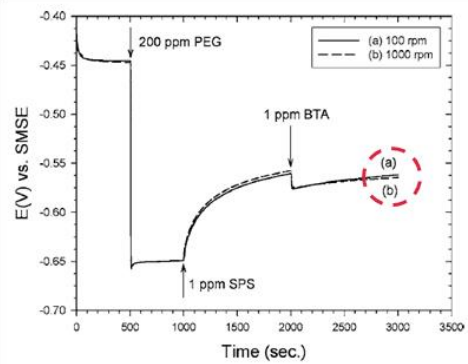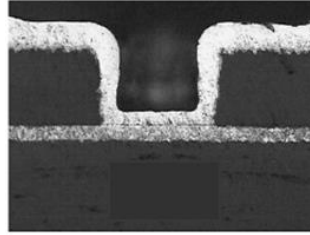
Figure 1.9. Microvia filling performance and potential profiles with the injection orders

of additives: (a) JGB and (b) BTA. (Ref. 48)

< Leveler >

Chemical name	Molecular structure
Janus Green B (JGB)	
Diazine Black (DB)	
Alcian Blue	
Safranin T	

Figure 1.10. Representative dye–type levelers for Cu electrodeposition.

1.5. Purpose of this study

In this study, newly synthesized triethylene glycol (TEG)–based levelers are examined to develop levelers showing the effective inhibition effect for bottom–up filling of microvia. Although TEG–based leveler with iodide ion (I^-) shows the strongest inhibition in a previous report, the faradaic efficiency of I^- is lower than that of Br– because the formation of CuI induce the charge loss by the electrochemical reaction. For the above reasons, Br^- is attracting the attention as the alternative ion. Before the application as the counter ion of TEG–based levelers, the interactive effects between Br^- and additives were studied. Br^- showed the synergistic inhibition with the suppressor and resulted in bottom–up filling without any organic levelers in the optimum range of concentration ratio between Br^- and SPS.

Based on the results, Br^- was selected as the counter ion in all synthesized levelers for microvia filling. In order to compensate the weakened inhibition effect by Br^-, we investigated whether structural modification of TEG–based levelers enhanced the inhibition effect. First, the effect of terminal functional groups (allyl, propyl, benzyl, and naphthylmethyl) in TEG–based levelers were examined. It was confirmed that the inhibition effect of levelers with aromatic ring groups became stronger, and the degree

of deactivation by SPS was found to be different. Second, TEG–based levelers according to the number of ammonium groups also were examined to enhance the inhibition effect. The adsorption strength of levelers with many ammonium groups was stronger, and they showed an additional inhibition effect through the interaction with SPS. As a results, bottom–up filling of microvias was obtained by using the structurally improved synthetic levelers, indicating the lower top thickness and the higher speed filling.

CHAPTER II

Experimental

2.1. Electrochemical analyses

The standard Cu electrolyte consisted of 0.92 M $CuSO_4 \cdot 5H_2O$ (99% purity, SEO AN CHEM TEC), 0.43 M H_2SO_4 (95% purity, DAEJUNG), and 0.82 mM HCl (35% purity, DAEJUNG). All experiments, such as electrochemical analyses and microvia filling, used the standard Cu electrolyte.

Linear sweep voltammetry (LSV) and chronopotentiometry were conducted using a potentiostat (PAR 263, EG&G Princeton Applied Research Corp.). A three–electrode system consisting of a Cu rotating disk electrode (RDE, geometric area = 0.07 cm^2) as the working electrode, a Cu wire as the counter electrode, and KCl–saturated Ag/AgCl as the reference electrode was used for the electrochemical analyses, as shown in Fig. 2.1. Before each measurement, the Cu RDE was mechanically polished using a sandpaper (2000 grit) to obtain a smooth and reproducible Cu surface and washed with deionized water to achieve same initial conditions. The rotating speed of the Cu RDE was controlled to 100 and 1000 rpm to replicate the convective motion of the electrolyte

at the bottom and top of the microvias, respectively. LSV was performed by sweeping the potential from 150 to –350 mV (vs. Ag/AgCl) at a scan rate of 1 or 10 mV/s. Tafel plots were obtained from LSV curves scanning at a scan rate of 1 mV/s. EIS analyses in Section 3.2 were performed with a PAR 2273 (EG&G Princeton Applied Research Corporation) in the range of 100 kHz to 15 Hz and the amplitude at 5 mV. Chronopotentiometry was performed at a current density of 15 mA/cm^2 over the course of 60 min. In Section 3.3, the current density increased to 30 mA/cm^2 to investigate the effect of additives in high current density condition.
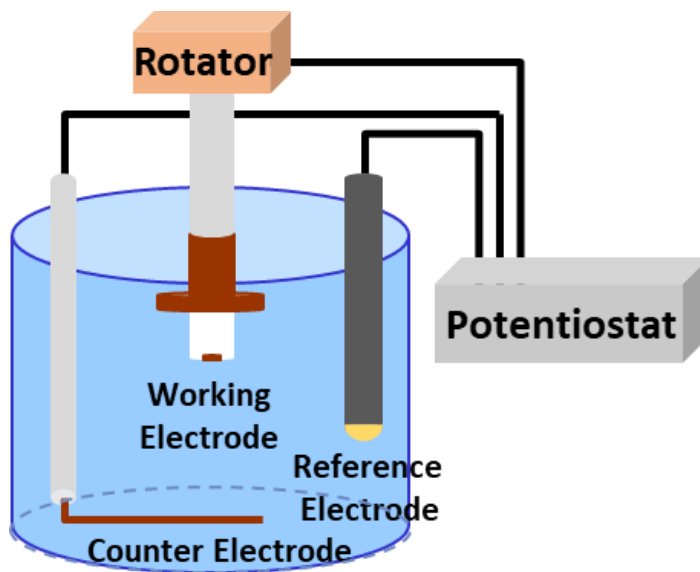
Figure 2.1. Schematic diagram of electrochemical analysis cell with three electrodes system for the Cu electrodeposition.

2.2. Microvia filling

Microvia filling experiments were carried out on PCB (2.1 cm × 2.2 cm) substrate supplied by Samsung Electro–Mechanics Co. Ltd. The dimensions of microvias were 130 and 100 μm in width at the top and bottom, and 100 μm in depth. The distance between each vias (1750 per substrate) was about 300 μm. The de–smear process eliminated the laminate fragments and improved the adhesion of the Cu seed layer which uniformly covered the PCB substrate. Fig. 2.2 showed the microvia filling cell with the circulation and nozzle system. The electrolyte in a polypropylene bath was ejected onto the PCB substrate through nozzles for via filling. The temperature of the Cu plating solution was maintained by the external cooling system at 25 °C. The PCB substrate and IrO_2/Ti plate covered by a proton–conducting membrane were used as the cathode and anode, respectively. Microvia filling was commonly performed at 15 mA/cm^2 for 60 min or 30 mA/cm^2 for 30 min in the Cu plating solution containing additives. The electrodeposition time was changed to confirm the filling mechanism according to the additive compositions. After the filling process, samples were embedded in an acrylic resin, and then mechanically ground using silicon carbide abrasive disks (P240, P600, P1200, and P4000 in sequence) and polycrystalline diamond suspension (average

diameter = 1 μm). The cross–sectional images of microvias were observed with an

optical microscope (ICS–306B, SOMETECH). On average, 30 microvias/substrate were

examined to check the filling profile of the Cu deposited in the microvia.
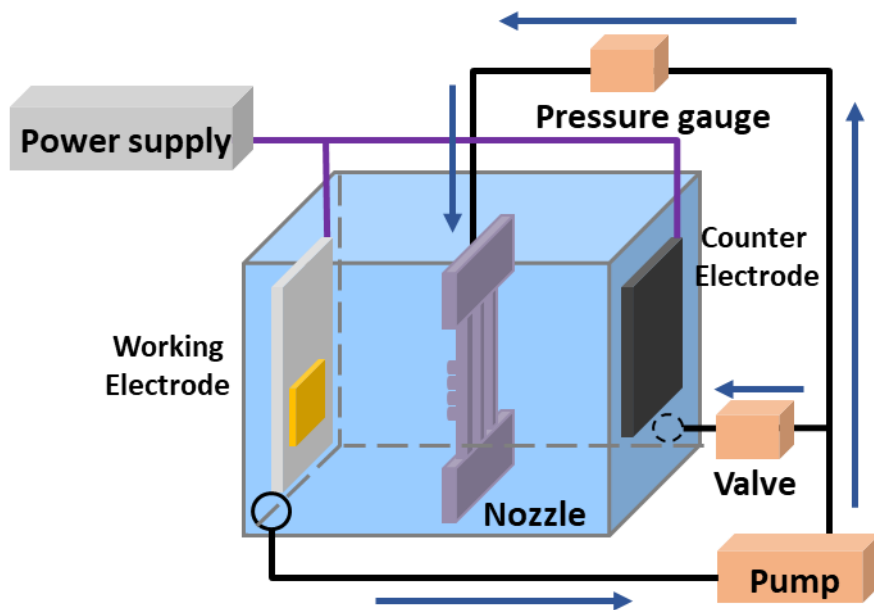
Figure 2.2. Schematic diagram of flow cell with two electrodes system for Cu microvia

filling.

2.3. Additives for microvia filling

SPS was adopted as the accelerator in all experiments. The concentrations of SPS were varied from 3 to 60 μM. PEG (average molecular weight = 1500) and PPG–PEG–PPG (average molecular weight = 2000) were used as the suppressor. The concentration of suppressors was fixed at 100 μM. NH_4Br was applied as the Br^- source in Section 3.1. In order to confirm the effective concentration range, the concentration of Br^- was changed from 50 to 400 μM.

In Section 3.2 and 3.3, TEG-based levelers were synthesized by Yoonjae Lee in prof. Young Gyu Kim's group. The detailed synthetic procedures and molecule analyses were explained in Appendix II and III. The synthesized levelers were devised considering three structural components as shown in Fig. 2.3. First, the quaternary ammonium groups with halide counter ions were selected. The positive charge of ammonium groups impeded the reduction of copper ions adsorbing on the Cu surface,[53,56,59] which are considered to be beginning of convection–dependent adsorption behavior. Second, the ethylene glycol unit, which is the monomer unit of most generally utilized suppressor, PEG, was adopted. The ethylene glycol unit was expected to enhance the adsorption intensity of levelers compared to those without this unit. Third, hydroxyl groups were

positioned on both sides of the carbon chain. The electron rich oxygen of hydroxyl group was expected to participate in the formation of inhibition layer of hydroxyl–Cu^+–Cl complexes.

TEG–based levelers varying the terminal functional groups were synthesized through the synthetic scheme in Fig. 2.4. They have different terminal functional groups: ally groups (Lev 1), propyl groups (Lev 2), benzyl groups (Lev 3), and naphthylmethyl groups (Lev 4). And TEG–based levelers according to the number of quaternary ammonium groups were also synthesized through the synthetic scheme in Fig. 2.5. The synthesized levelers were named according to the number of quaternary ammonium groups: Lev A–1 (one ammonium groups in Fig. 2.5. (a)), Lev A–2 (two ammonium groups such as Lev 1 in Fig. 2.4), and Lev A–3 (three ammonium groups in Fig. 2.5. (b)). All synthesized levelers were used in the fixed concentration of 7 μM.
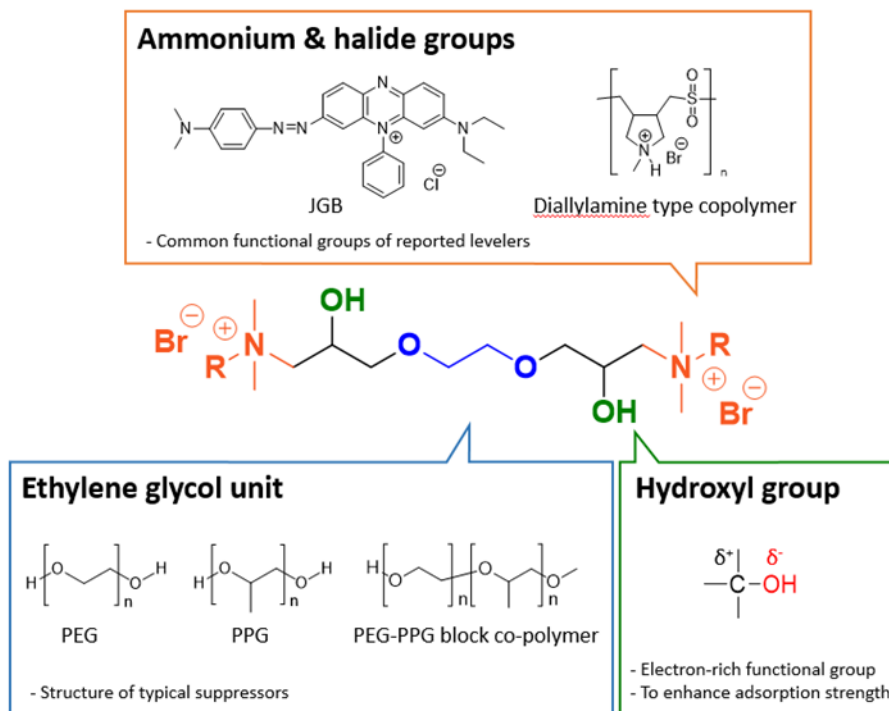
Figure 2.3. Three structural components of the synthesized levelers.
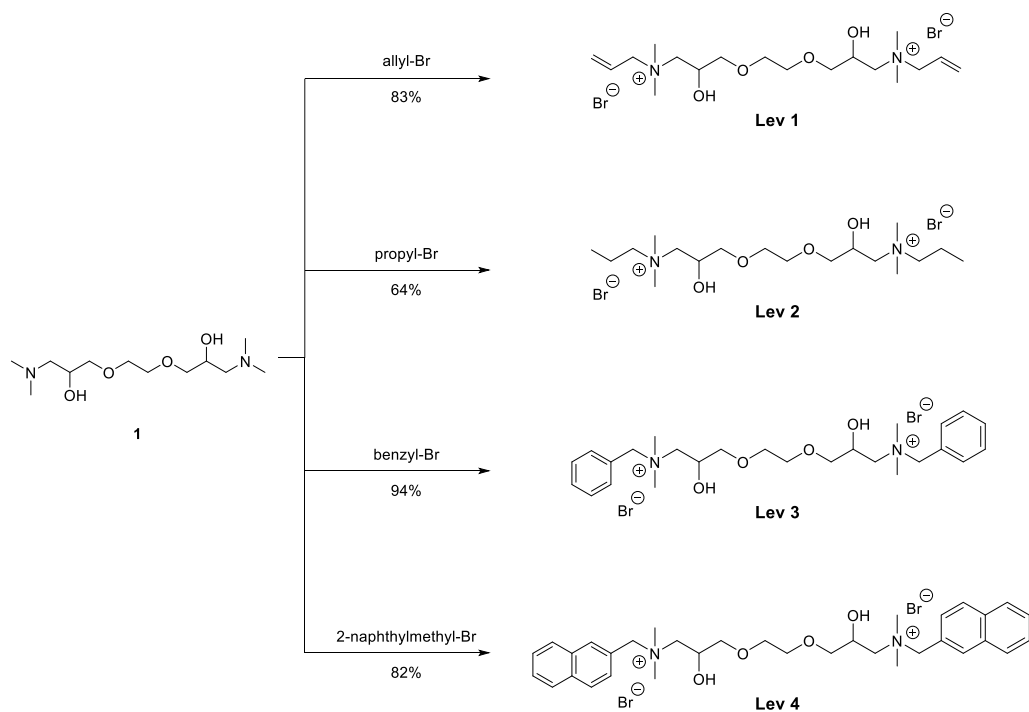
Figure 2.4. Schematic diagram of synthetic route for TEG–based levelers containing different terminal functional groups.
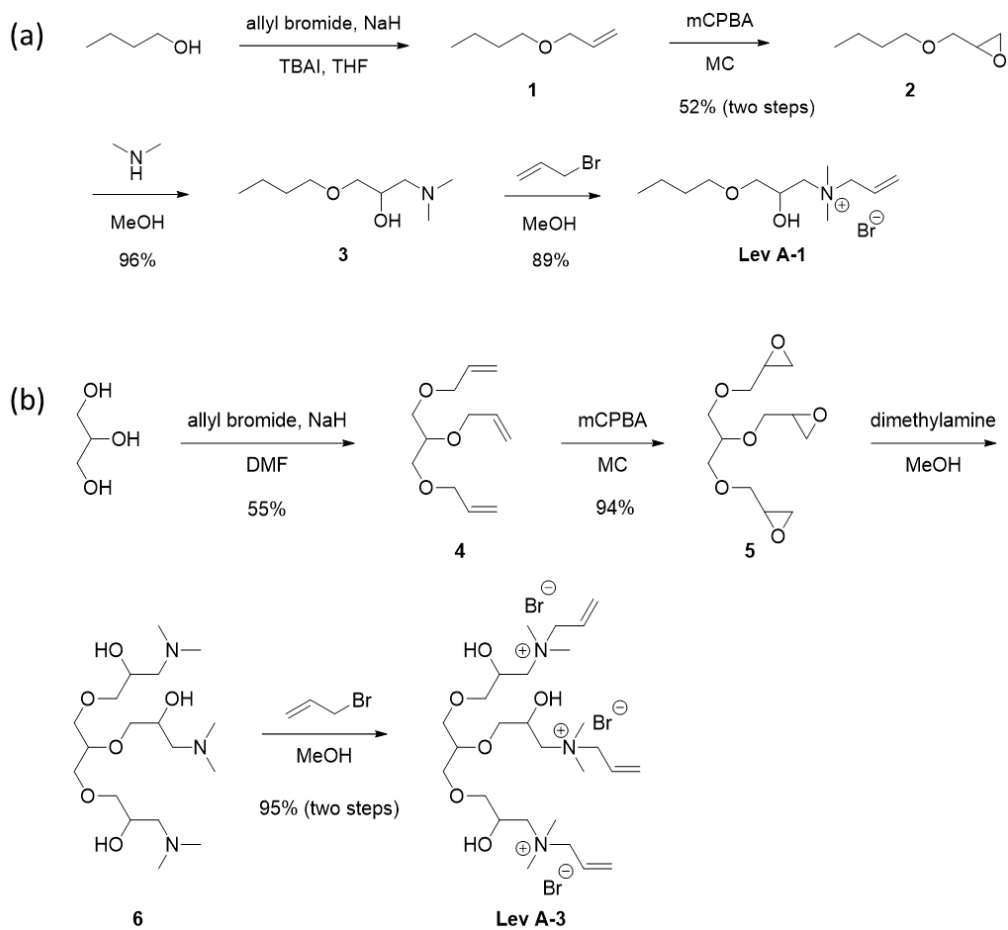
Figure 2.5. Schematic diagram of synthetic route for TEG–based levelers according to the number of ammonium groups: (a) Lev A–1 (one–ammonium group) and (b) Lev A–3 (three–ammonium groups).

CHAPTER III

Results and Discussion

3.1. Bromide ions as the additive in microvia filling

Halide ions such as I⁻ and Br⁻ have been reported as additives for TSV filling.[28,51,61,62] Unlike Cl⁻, I⁻ and Br⁻ form immobilized Cu–I and Cu–Br species by chemisorption,[63,64] which are stable enough (a lower solubility of Cu–I and Cu–Br compared to Cu–Cl complex) to interrupt the charge transfer process on the Cu surface. It was also reported that the bottom–up filling rate with Br⁻ is higher than that achieved with I⁻, even though Br⁻ suppresses Cu deposition less effectively than I⁻.[65] High–speed TSV filling can be achieved by using Br⁻ for Cu electrodeposition with high current efficiency (~88%), instead of I⁻ (~31%).[65] As a results, Br⁻ is suitable to via filling as an additive instead of I⁻. For the reasons, the additional studies are necessary to confirm how Br⁻ interact with accelerator and suppressor and how the competitive adsorption between additives and Br⁻ affects the Cu filling performance in microvia.

3.1.1. Electrochemical behaviors of bromide ions and interaction with SPS.

LSV was first performed to investigate the interaction between PEG and Br⁻ at two electrode rotating speeds in Fig. 3.1. Two rotating speeds were used to facilitate comparison of the results of the electrochemical analyses with the microvia filling performance analysis because the electrode rotating speeds of 100 and 1000 rpm replicate the fluidic motions at the bottom and top of the microvias, respectively.[23,48] Fig. 3.1 (a) shows that the adsorption of Br⁻ inhibited Cu electrodeposition. The onset potential for Cu ion reduction was confirmed as 110 mV (vs. Ag/AgCl) in the existence of Cl⁻, and it was negatively shifted to –55 mV when Br⁻ was added. However, the inhibitory effect of Br⁻ was much weaker than that of PEG+Cl⁻ because PEG and Cl⁻ formed a suppression layer of PEG–Cu⁺–Cl⁻ or PEG–Cl⁻. Interestingly, when Br⁻ was present with PEG, the suppression effect was improved relative to that achieved with PEG+Cl⁻ or Br⁻ individually, which agrees with previous studies reporting the enhancement of suppression by adding Br⁻ to PEG.[66,67] The onset potential for the PEG+Br⁻ system was approximately –255 mV, compared to –130 mV for PEG+Cl⁻. This result suggests that the adsorbed Br⁻ and PEG interacted with each other. A previous

study using Raman spectroscopy indicated that Cl^- adsorbed on the surface of Cu binds

with Cu^+ produced by Cu ion reduction (i.e., $Cu^{2+} + e^- \rightarrow Cu^+$), and the dangling Cu^+

ions were covered by interaction with two oxygen atoms of the PEG molecules.[37] The

Br^- ions are also able to coordinate with Cu^+ [68]; therefore, it is possible that the Br^- ions

form suppression layers with PEG in the same manner as the Cl^- ions. Because Br^- ions

were immobilized on the Cu surface by the stronger adsorption compared to Cl^-, the

inhibitory effect of PEG with Br^- was stronger than that of PEG–Cl^-, as shown in Fig.

3.1 (a). The suppression effect followed the same trend when the electrode rotating speed

was increased to 1000 rpm (Fig. 3.1 (b)). Although it is necessary to clarify the

adsorption structure of PEG and Br^- by other analytical tools including surface–

enhanced infrared absorption spectroscopy (SEIRAS), [69] raman spectroscopy,[37] and

secondary–ion mass spectrometry (SIMS),[70] these electrochemical results indicate that a

combination of PEG and Br^- induced the strongest suppression. Note that forced

convection did not increase the suppression effect of PEG–Br^- (Figs. 3.1 (a) and 3.1 (b)),

meaning that the Cu surface was fully covered by the PEG–Br^- suppression layer,

regardless of the electrode rotation speeds. Considering this phenomenon, it is expected

that the combination of PEG and Br^- without accelerators could not induce Cu bottom–

up filling at the microvias because this combination will deactivate all Cu surfaces regardless of the positions in the microvias.

We further investigated the interaction between PEG–Br⁻ and SPS by LSV (Fig. 3.2) and chronopotentiometry (Fig. 3.3). Fig. 3.2 shows the voltammograms with varying SPS concentrations at a fixed concentration of PEG and Br⁻. At the electrode rotating speed of 100 rpm (Fig. 3.2 (a)), the addition of SPS to PEG–Br⁻ clearly resulted in depolarization and increased the current density for Cu electrodeposition. In particular, the current density increased from –8.7 to –96 mA/cm^2 (Fig. 3.2 (a)) at –200 mV when the SPS concentration increased from 0 to 48 μM. However, at an electrode rotating speed of 1000 rpm (Fig. 3.2 (b)), SPS addition did not cause a remarkable increase in the current density. At an electrode potential of –200 mV, the current density increased by only –24.4 mA/cm^2 after adding 48 μM SPS. These results suggest that the effect of SPS on PEG–Br⁻ depends on the fluidic motions near the Cu surface, and the strong forced convection inhibited detachment of the PEG–Br⁻ suppression layer by SPS. These results are primarily attributed to the changes in the flux of Br⁻ to the Cu surface under convection. The increase in the suppression with the Br⁻ flux was also observed in the additional LSV with varying a scan rate (not shown here). In the presence of PEG–Br⁻ and SPS, the stronger suppression was observed at a lower scan rate because a lower

scan rate provides a longer time for the Br⁻ to reach the Cu surface. A previous study indicated that the Cl⁻ flux to the Cu surface determines the extent of surface coverage achieved with the PEG–Cl⁻ layer relative to that covered by SPS [22]. Forced convection increased the Cl⁻ flux, which reinforced the formation of PEG–Cu⁺–Cl⁻ layers, eventually leading to a decrease in the SPS surface coverage. Because the Br⁻ concentrations examined in this study were extremely low compared to the concentration of Cl⁻ in conventional electrolytes for Cu electrodeposition, the effect of Br⁻ flux (i.e., forced convection) on controlling the surface coverage of the suppression layer and accelerator would become more significant.

Fig. 3.3 shows the time–dependent competitive adsorption of Br⁻ and SPS with varying electrode rotation speeds and concentrations of SPS and Br⁻. In general, at a fixed current density of 15 mA/cm^2, the electrode potentials shifted in the positive direction. This positive shift was caused by displacement of the adsorbed PEG–Br⁻ by SPS, similar to the displacement of pre–adsorbed PEG–Cl⁻ by SPS.[11] Figs. 3.3 (a) and 3.3 (b) show the change in the electrode potential with increasing concentration of Br⁻ at the electrode rotating speeds of 100 and 1000 rpm, respectively. When weaker forced convection was applied, the electrode potential was positively shifted at all Br⁻ concentrations. It was also verified that the displacement of SPS was facilitated at a

lower concentration of Br⁻, observed as a relatively quicker increase in the electrode potential. In contrast, at 1000 rpm, the electrode potentials remained the same for 60 min, except in the case with the lowest Br⁻ concentration (50 μM). The constant potential maintained for 60 min suggests that SPS could not displace the adsorbed PEG–Br⁻ suppression layers. Adsorption of SPS with detachment of the PEG–Br⁻ suppression layers could take place when the Br⁻ concentration was lower than 50 μM. Comparison of the results obtained at the two electrode rotating speeds highlights that strong forced convection enhanced the adsorption of PEG–Br⁻, preventing the adsorption of SPS.

   Similar behavior was observed in Figs. 3.3 (c) and 3.3 (d), which shows the chronopotentiometry data with increasing concentrations of SPS. Fig. 3.3 (c) shows that the addition of more SPS facilitated the displacement of the PEG–Br⁻ suppression layer. The incubation time preceding the positive shift in the electrode potential became shorter with increasing SPS concentration. At the SPS concentration of 48 μM, the potential shift was completed in 10 min, while it was continued for 50 min at the SPS concentration of 12 μM. However, when stronger convection was applied (Fig. 3.3 (d)), the displacement of SPS declined significantly, observed as a slower shift of the electrode potential regardless of SPS concentrations. As explained above, this

phenomenon resulted from the enhanced adsorption of the PEG–Br⁻ suppression layers as the forced convection increased the flux of Br⁻ to the Cu surface.

Interestingly, the oscillation of electrode potential was observed in Figs. 3.3 (a) and 3.3 (c). Previous studies suggested that the potential oscillation during a chronopotentiometry was caused by a repetitive change in the surface coverage of organic additives,[71,72] the breakdown and reconstruction of additive layers,[73] and the alternative formation and dissolution of an organic leveler–Cu⁺–MPS suppressor ensemble.[74] Besides, it was reported that the oscillatory behavior was observed in the presence of accelerators and organic levelers without polymeric suppressors, and also affected by the concentration of Cl⁻ ions.[73] In this study, the potential oscillation was observed at a lower electrode rotating speed of 100 rpm, suggesting that the oscillation was caused under a lower flux of Br⁻ ions. The oscillation occurred after the potential shift was completed, meaning that the oscillation took place when the Cu surface was mostly covered by SPS. Although it is difficult to conclude the mechanism of the potential oscillation observed in Figs. 3.3 (a) and 3.3 (c), the results suggested that the potential oscillation might be due to a repetitive process of the breakdown of SPS adlayer by Br⁻ ions and re–adsorption of SPS on the Cu surface. Although it was reported that this oscillation behavior of electrode potentials caused the change in the grain size and

microstructure of Cu deposits,[72,75] further research is necessary to clarify how this behavior affects gap–filling performance.

Figs. 3.2 and 3.3 indicate that the competitive adsorption between SPS and PEG–Br$^-$ depended on the concentrations of SPS and Br$^-$ and the forced convection. An increase in the Br$^-$ (or SPS) concentration interrupted (or facilitated) the displacement of the PEG–Br$^-$ layers with SPS. Forced convection enhanced the formation of PEG–Br$^-$ suppression layers, which effectively inhibited the adsorption of SPS. With regard to microvia filling, these results suggest that the SPS to Br$^-$ concentration ratio should be carefully determined to maximize the bottom–up filling performance. Therefore, microvia filling was performed by varying the concentration of SPS and Br$^-$ to investigate how the competitive adsorption between SPS and PEG–Br$^-$ affects the bottom–up filling of Cu in microvias.
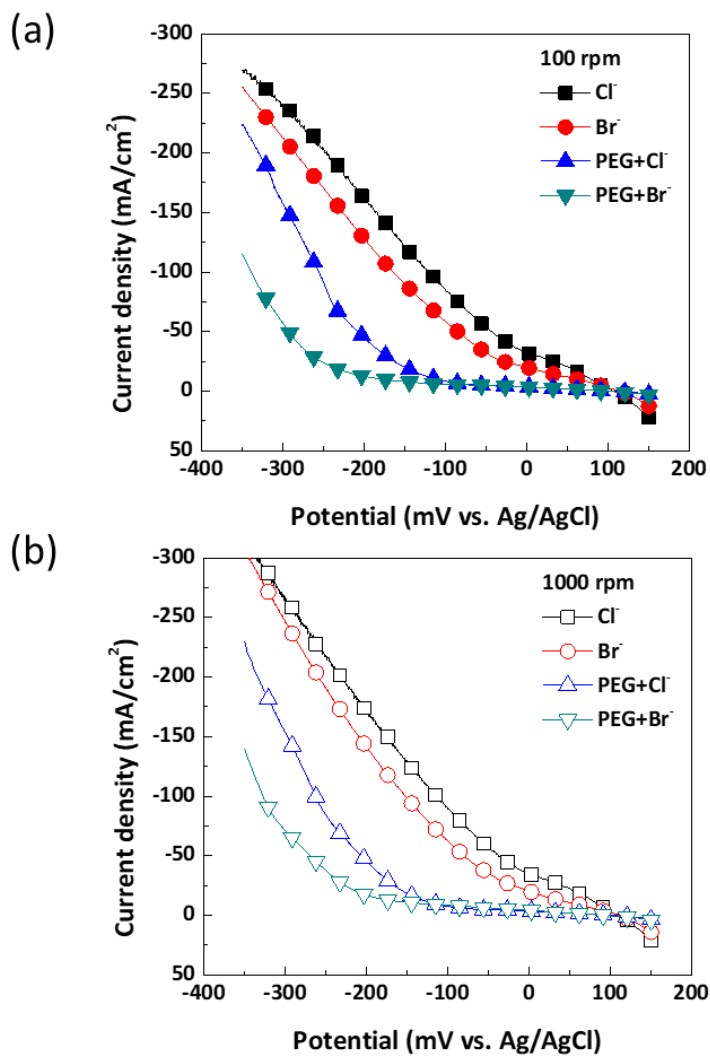
Figure 3.1. LSV plots for the reduction of copper ions with various combinations of additives at the rotating speed of (a) 100 and (b) 1000 rpm. The concentrations of PEG and halide ions (Cl⁻ and Br⁻) were 100 and 820 μM, respectively.
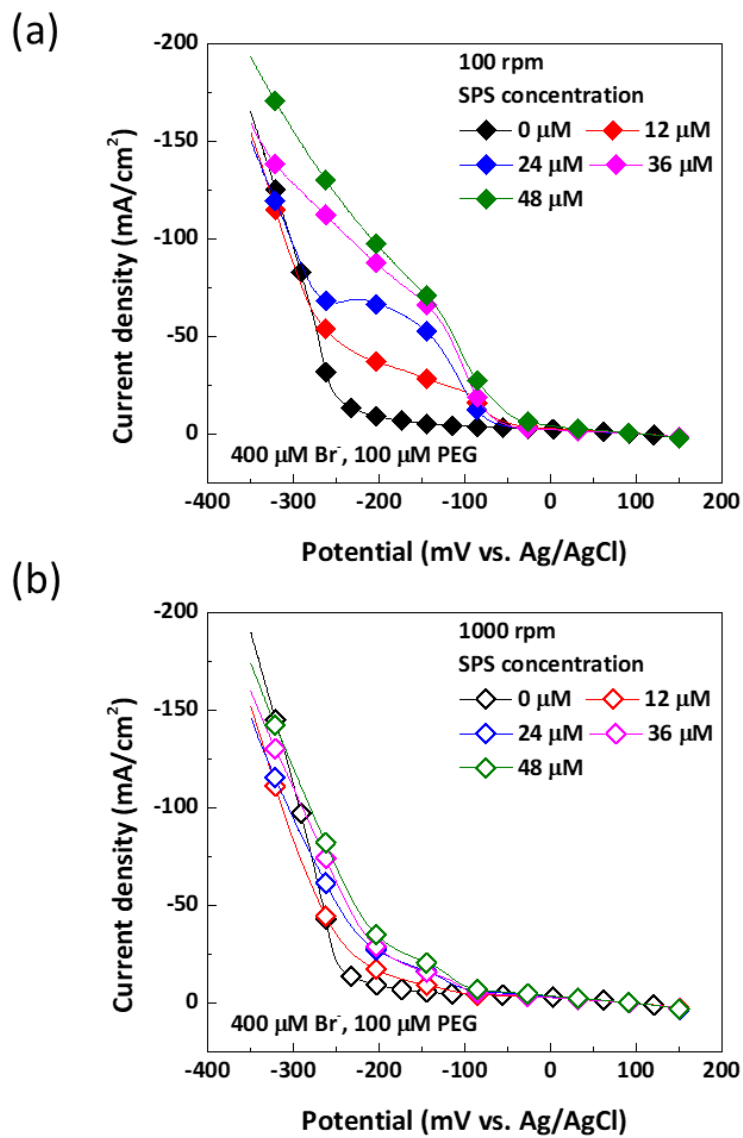
Figure 3.2. LSV plots for the reduction of copper ions changing the concentration of SPS in the presence of PEG and Br⁻ at (a) 100 and (b) 1000 rpm. The concentrations of PEG and Br⁻ were 100 and 400 μM, respectively.
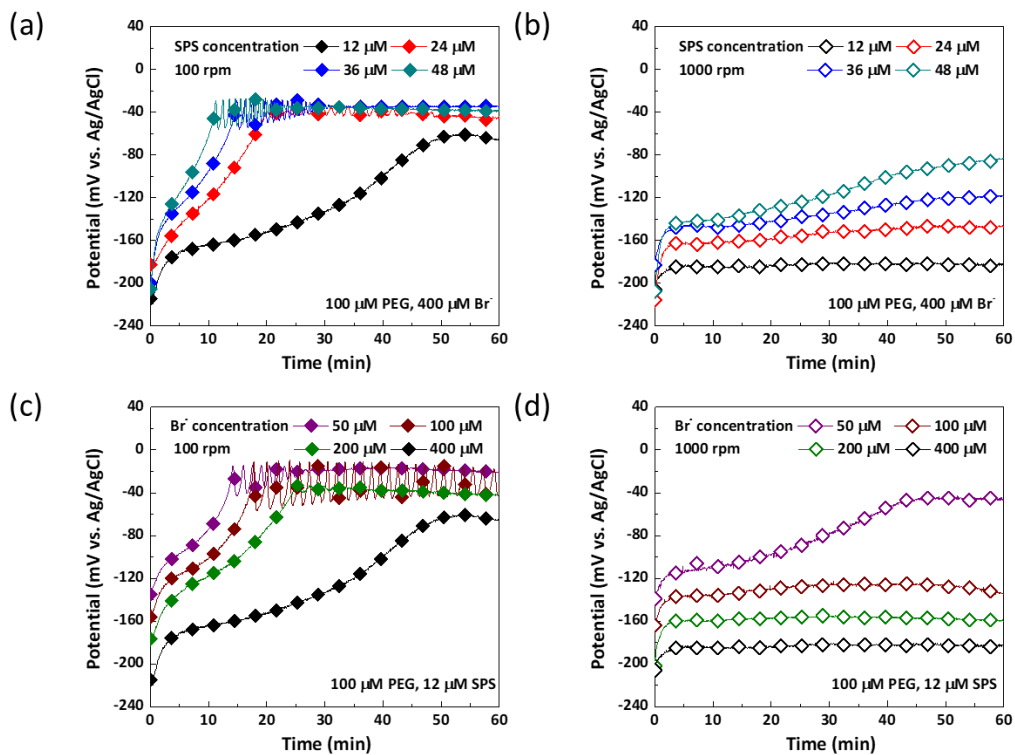
Figure 3.3. Chronopotentiometry results obtained by the current density of -15 mA/cm^2 with changing the concentration of (a), (b) Br$^-$ and (c), (d) SPS in the presence of PEG. Electrolytes of (a) and (b) consisted of 12 μM SPS, and electrolytes of (c) and (d) consisted of 400 μM Br$^-$. The rotating speed was (a), (c) 100 and (b), (d) 1000 rpm.

3.1.2. Microvia filling varying the concentration of Br⁻ and SPS

The cross–sectional profiles of Cu filling with varying concentrations of SPS and Br⁻ are shown in Fig. 3.4. As expected, the SPS to Br⁻ concentration ratio had a significant impact on the filling performance. When the concentration of SPS was relatively high (upper–right corner in Fig. 3.4) or the concentration of Br⁻ was relatively high (lower–left corner in Fig. 3.4), V–shaped filling profiles were observed, indicating negligible bottom–up characteristics. The green–dotted box indicates the conditions for obtaining defect–free filling without dimples. Note that a dimple is defined as a concave profile at the top of the microvias, having a depth exceeding 5 μm.[27] The conditions in the first column and the first row were the same as those adopted for chronopotentiometry in Figs. 3.3 (a) and 3.3 (c), respectively. Considering both the electrochemical results and filling profiles, it can be concluded that to achieve dimple–free Cu filling, at 100 rpm, SPS displacement (i.e., activation for Cu electrodeposition inside the microvias) should be completed in 20 min, and at 1000 rpm, the strong passivation layer (i.e., PEG–Br⁻ suppression layers at the top surface of PCBs) should be maintained for at least 20 min. Using 100 μM Br⁻ and 12 μM SPS, one of these criterion was not met.

The filling performance of microvias was quantitatively analyzed by assessing the ratio of the Cu thickness at the top surface and that at the bottom of the microvias, that is, the thickness ratio (%) = $T_{bottom}/T_{top} \times 100$. Fig. 3.5 (a) presents the changes in the thickness ratio according to the concentrations of Br$^-$ and SPS. Similar to the green–dotted box in Fig. 3.4, the thickness ratio was higher in the diagonal direction, suggesting that the concentration ratio between the two additives determines the bottom–up filling characteristics. The importance of the concentration ratio is further highlighted in Fig. 3.5 (b), which shows the volcano shape of the bottom–up filling performance plot. It is clear that bottom–up filling (i.e., a thickness ratio > 275%) can be achieved at concentration ratios ranging from 0.2 to 0.7. It can be hypothesized that within this concentration ratio range, the PEG–Br$^-$ suppression layers effectively passivated the top surface of the PCB substrates, while SPS selectively promoted Cu electrodeposition inside the microvias. To verify this hypothesis, the cross–sectional profiles at different filling stages were investigated for three representative cases: excess SPS (Fig. 3.6 (a)), excess Br$^-$ (Fig. 3.6 (b)), and optimum SPS and Br$^-$ (Fig. 3.6 (c)).

As shown in Fig. 3.6 (a), when excess SPS was introduced, Cu electrodeposition was initially concentrated at the bottom corners of the microvias, marked with a white arrow, forming softly curved profiles. This profile was mainly influenced by the accumulation

of SPS due to area reduction at the bottom corners of the microvias, as described in the CEAC model.[43,76] However, at the same time, Cu was vigorously electrodeposited outside the microvias, impeding the bottom–up Cu filling. In contrast, when the Br^- concentration was relatively high, sharp deposition profiles appeared at the bottom corners of the microvias (white arrow in Fig. 3.6 (b)). This profile, resulting from conformal deposition, suggests that SPS cannot induce selective acceleration of Cu deposition because the strong suppression layer formed with PEG was maintained by the excess Br^- and could not be displaced by SPS. Conformal deposition continued for 1 h, supporting that the surface coverage of SPS and PEG–Br^- did not change at all positions of the via during Cu electrodeposition. Fig. 3.6 (c) shows the filling profiles with the optimum concentration ratio of SPS and Br^-. The white arrow in Fig. 3.6 (c) highlights the smooth curved profile resulting from the accumulated SPS due to area reduction. By comparing the profiles at 60 min, it was confirmed that less Cu was deposited at the top corners compared to the cases with excess SPS or Br^-. These results indicate that Cu electrodeposition started at the bottom corners and then filled the microvias, effectively inhibiting Cu deposition at the top surface, as hypothesized above.

In summary, the effect of Br^- on the adsorption of PEG and SPS was investigated by electrochemical analyses and microvia filling. The addition of Br^- in the electrolyte

containing PEG remarkably improved the inhibition effect for Cu deposition, suggesting that Br⁻ stabilized the inhibition layer of PEG on the Cu surface. This inhibition layer composed of PEG and Br⁻ retarded the adsorption of SPS. The concentration of Br⁻ and SPS, and the forced convection affected the competitive adsorption between the inhibition layer of PEG–Br⁻ and SPS. As a results, we could know that the optimum concentration ratio should be applied for Cu bottom–up filling of microvias. In the presence of excess Br⁻ (or SPS), PEG–Br⁻ layers (or SPS) dominantly covered all Cu surface, which induce the conformal filling. On the contrary, the optimum concentration ratio of SPS and Br⁻ results in the selective Cu deposition at the bottom of microvias (i.e., SPS dominant) while inhibiting Cu deposition outside microvias (i.e., PEG–Br⁻ dominant). The relationship between the concentration ratio of additives and filling performance of microvias would be helpful in improving the industrial electrodeposition processes, and it could be useful for developing new leveler composed of Br⁻ as the counter ion.
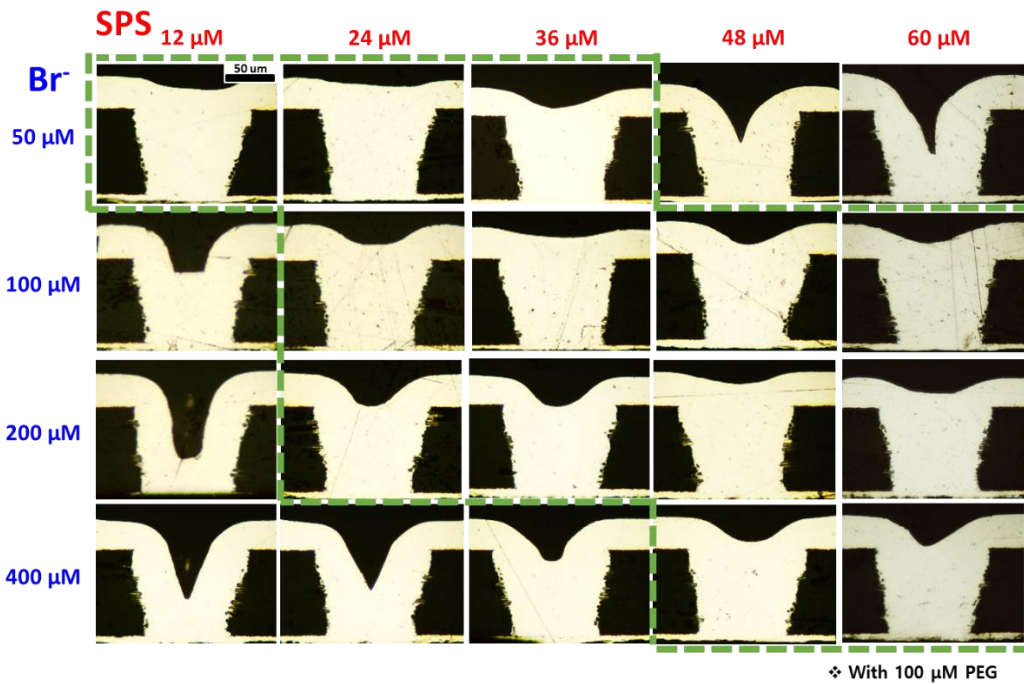
Figure 3.4. Cross–section images of microvias with varying concentrations of Br⁻ and SPS in the presence of 100 µM PEG. The current density was –15 mA/cm^2; filling time was 90 min (i.e., 81 C/cm^2). The green–dotted box indicates the conditions for obtaining defect–free filling without dimples (the depth of a concave profile at the top of microvias < 5 µm).
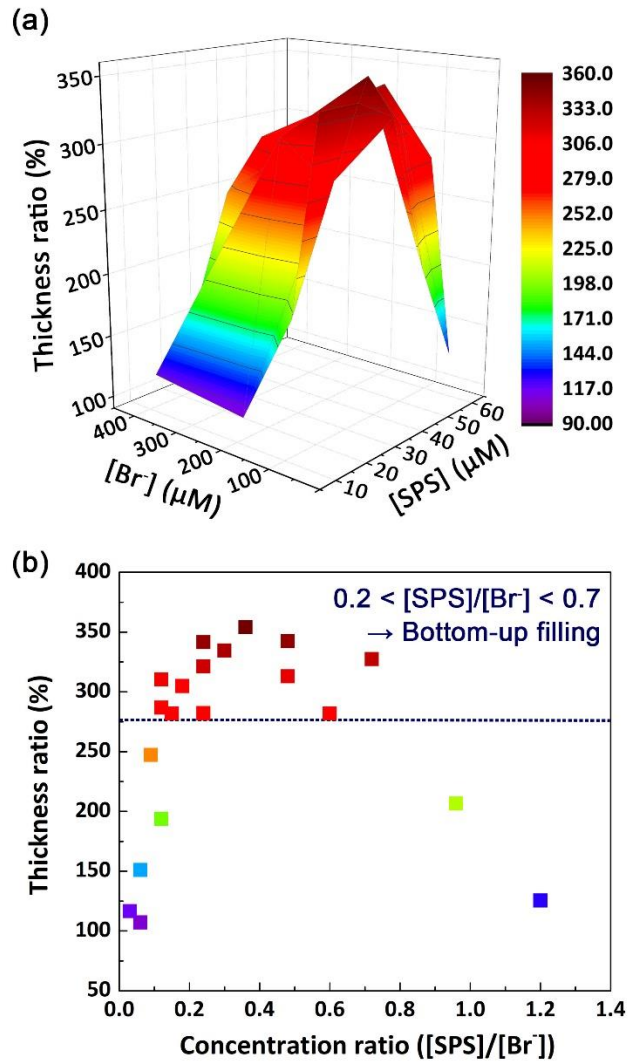
Figure 3.5. (a) Filling performance of microvias as a function of the concentrations of Br⁻ and SPS. (b) Thickness ratio as the filling performance according to the concentration ratio of SPS and Br⁻ ([SPS]/[Br⁻]). All results were obtained from the filling profiles shown in Fig. 3.4.
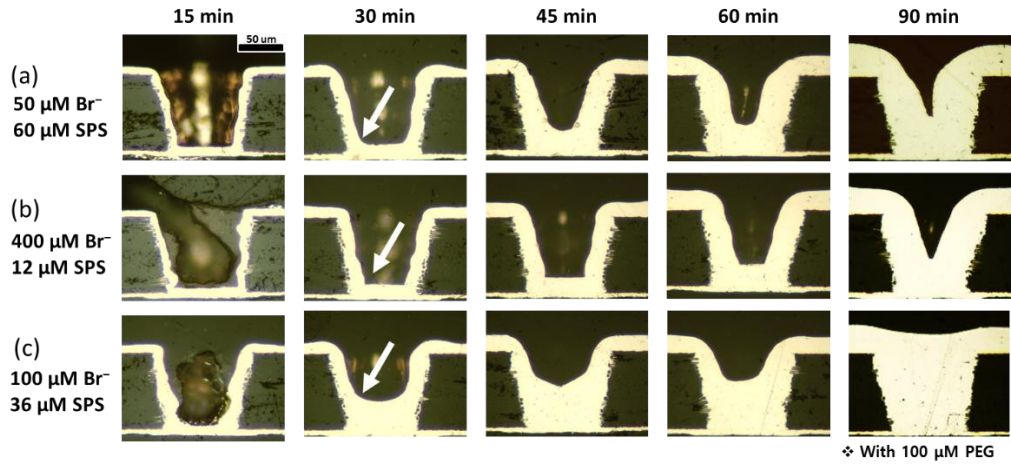
Figure 3.6. Cross–sectional images according to the electrodeposition time with three additive combinations: (a) 60 µM SPS+50 µM Br⁻ (concentration ratio = 1.2), (b) 12 µM SPS+400 µM Br⁻ (ratio = 0.03), and (c) 36 µM SPS+100 µM Br⁻ (ratio = 0.36). The concentration of PEG was fixed at 100 µM, and the current density was −15 mA/cm².

3.2. Terminal functional groups of levelers

In Section 3.1, Br⁻ was verified as an additive for microvia filling by Cu electrodeposition. Br⁻ was effective to form the interaction with the suppressor more than Cl⁻ and I⁻. However, the longer deposition time (90 min) is necessary to make bottom–up filling. Only Br⁻ was not enough to completely replace the organic leveler even though Br⁻ has a strong interaction with additives to inhibit the reduction of Cu. For the reason, we displaced I⁻ to Br⁻ as the counter ion in TEG–based levelers. The inhibition effect of organic levelers decreased by displacing I⁻ to Br⁻, as mentioned in the previous report.[61] Therefore, Organic structures of levelers should be modified to compensate for the insufficient inhibition. First, the inhibition of TEG-based levelers was changed by varying terminal functional groups.

The synthesized levelers contained different terminal functional groups: allyl groups (Lev 1), propyl groups (Lev 2), benzyl groups (Lev 3), and naphthylmethyl groups (Lev 4), as shown in Fig. 2.4. Comparing Lev 1 and Lev 2 would provide the information about the influence of π electrons of the allyl groups. Lev 3 was chosen to determine the influence of the aromatic groups which have the conjugated π–systems with a flat structure, thus providing a large adsorption surface. Lev 4 that include larger aromatic

systems than benzyl groups would clarify the influence on the size of aromatic systems. The structure–performance study of our synthesized levelers will aid the design of new levelers with the superior filling performance.

3.2.1. Inhibition effect with different terminal functional groups

The effect of the levelers on Cu electrodeposition was observed by LSV experiments as appearing in Fig. 3.7. The synthesized levelers were added into Std. Cu sol. to determine the effect of these single additives alone. Rotating speeds of 100 and 1000 rpm were selected to represent flow conditions at the bottom and top of microvias. Fig. 3.7 (a) showed that the onset potential at 100 rpm became negatively increasing from Lev 1 to Lev 4 in sequence, i.e., –8, –13, –43, and –59 mV, respectively. When the rotating speed increased to 1000 rpm, the further negative shift of the onset potential appeared like –23, –36 mV, –90, and –170 mV (Fig. 3.7 (b)). It is noticeable that the onset potential of Lev 2 did not much differ from that of Lev 1 at all rotating speeds, which means that the propyl and allyl terminal groups had nearly the same inhibition ability as levelers. On the other hand, the aromatic terminal groups had the stronger convection–dependent adsorption behavior since the difference values of onset potential

were measured to be 111 mV (Lev 4) and 47 mV (Lev 3). In the inhibition strength as the levelers, the aromatic terminal groups are found to be much effective, compared to aliphatic groups.

Additionally, the inhibition strength of the levelers was evaluated by determining the exchange current densities obtained by the Tafel plots (Fig. 3.8) using following equation.[77]

$$\log i = \log i_0 + \frac{-\alpha_c nF}{2.3RT}\eta \qquad [1]$$

Here, i_0, η, α_c, n, R, T, and F represent the exchange current density, the overpotential, the cathodic transfer coefficient, the number of electrons involved, the gas constant, the absolute temperature, and the Faraday constant, respectively. As listed in Table. 3.1, the exchange current densities were measured in the range from 0.40 to 2.30 mA/cm^2. The lowest one was found to be 0.40 mA/cm^2 in the case of Lev 4. Since the charge transfer resistance is inversely proportional to the exchange current density, EIS analysis was performed to compare the charge transfer resistances (Fig. 3.9). By applying the potential of –100 mV vs. OCP, the resistance values increased from 155.50 Ω in Lev 1 to 3152 Ω in Lev 4 (Table. 3.1). The synthesized levelers could be classified into three groups, and the naphthylmethyl group greatly enhanced the inhibition effect of leveler than benzyl groups.

The electrochemical analyses suggest that the aromatic groups have a considerable influence on the adsorption of the levelers on the Cu surface, leading to the strong inhibition of Cu reduction. In addition, the extended aromatic system of Lev 4 resulted in the greater inhibition than the other leveler. This significant enhancement of the inhibition effect is expected to be related to a nature of the aromatic ring system. Aromatic compounds are readily adsorbed on metal surfaces because of the conjugated planar ring structures with π–cloud and noncovalent interactions.[78,79] In addition, bigger hydrophobic part in the structure of additive seems to contribute the enhanced inhibition function.[80]

(a)

(b)
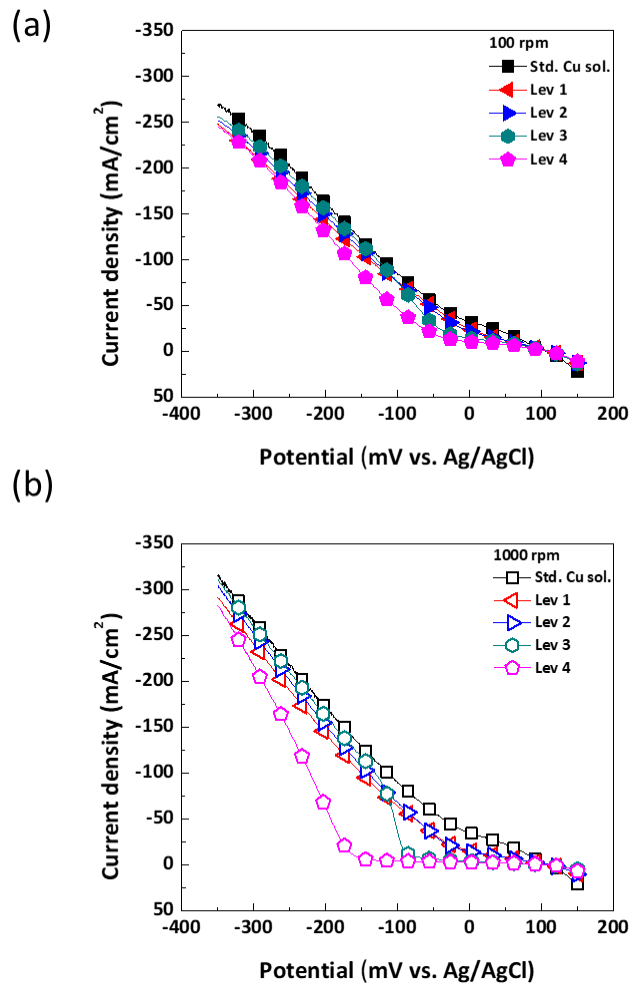
Figure 3.7. LSV plots for the reduction of copper ions in Cu electrolyte containing Lev

1, Lev 2, Lev 3, and Lev 4 obtained at (a) 100 and (b) 1000 rpm.
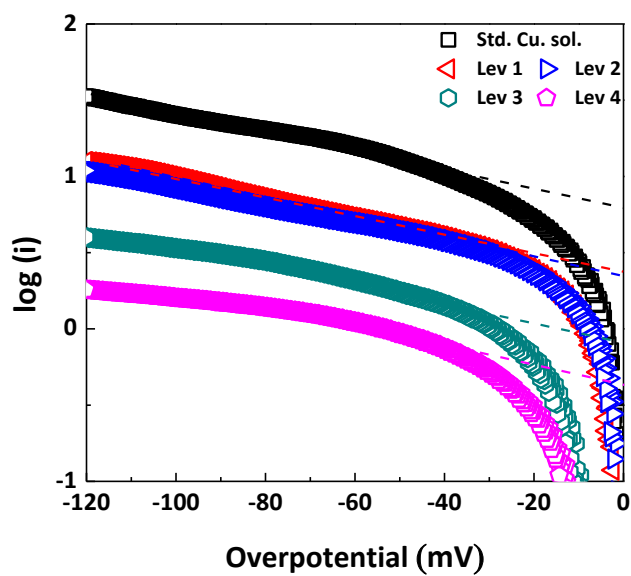
Figure 3.8. Tafel plots for the reduction of copper ions at 1000 rpm with and without

levelers: Lev 1, Lev 2, Lev 3, and Lev 4.
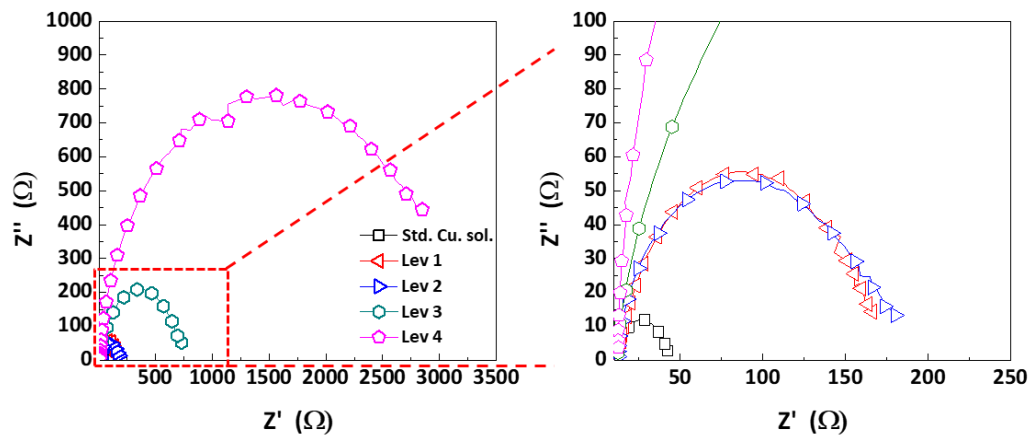
Figure 3.9. Nyquist plots measured in the Cu electrolyte at 1000 rpm with and without

levelers: Lev 1, Lev 2, Lev 3, and Lev 4.

Table. 3.1. Exchange Current Density, Cathodic Transfer Coefficient, and Charge

Transfer Resistance with and without Levelers: Lev 1, Lev 2, Lev 3, and Lev 4

	Tafel equation		Impedance
	$I_o(mA/cm^2)$	α_c	$R_{ct}(at\,-100\,mV)(\Omega)$
Std. Cu sol.	4.80(±0.42)	0.25(±0.01)	30(±1)
Lev 1	2.30(±0.07)	0.18(±0.01)	156(±5)
Lev 2	2.35(±0.12)	0.16(±0.01)	167(±3)
Lev 3	0.73(±0.03)	0.22(±0.01)	693(±35)
Lev 4	0.40(±0.02)	0.22(±0.01)	3152 (±12)

3.2.2. Interaction of levelers with the accelerator and the suppressor.

Fig. 3.10 depicted that the competitive adsorption between the leveler and SPS was measured through the potential shifts by changing injection orders of additives. When Lev 1 or Lev 2 was injected, the potential shifted negatively around –50 mV (Fig. 3.10 (a) and (b)). The further addition of SPS shifted the potential quickly to about –30 mV irrespective of the injection conditions. Lev 3 maintained the potential of about –80 mV, but it oscillated from –80 to –10 mV unlike aliphatic levelers when SPS were injected, as in Fig. 3.10 (c). These potential oscillations are considered to be the repeated construction and destruction of a complex layer between a certain additive and accelerator.[53,73,75] Therefore, this phenomenon that was similarly observed in other injection conditions might be related to the instability of the inhibition layer during the competitive adsorption between Lev 3 and SPS. On the other hand, Fig. 3.10 (d) represented that the potential of Lev 4 was found to be about –80 mV without any change regardless of the sequence of addition. These results means that the naphthylmethyl group of Lev 4 could withstand the deactivation by SPS unlike other functional groups.

The inhibition behavior of levelers could affect the complexed inhibition layer with the suppressor in filling process. Therefore, the deactivation of complexed inhibition

layer at top and bottom of via was described by the potential difference measurements in three–additive mixture (Fig. 3.11). The potential difference listed in Table. 3.2 is calculated by Eq. 2.

$$\Delta V = V_{100rpm} - V_{1000rpm} \tag{2}$$

For all the levelers, the potential at 100 rpm became positively increasing as time elapsed, as reported that Cl⁻ ions at weak forced convection interact predominantly with the accelerator in the same concentration of Cl⁻ ions even though these are essential for the complexed inhibition layer.[22] For the reason above, the slow supply of Cl⁻ ions at 100 rpm could lead to the collapse of inhibition layer, and then SPS species could easily accumulated on the Cu surface. The deactivation by SPS at 1000 rpm displayed the potential shift from –140 mV to about –90 mV in Lev 1, Lev 2, and Lev 3 mixture (Fig. 3.11 (a)–(c)). The potential oscillations of Lev 3 in Fig. 3.10 (c) were not observed because a stable inhibition layer was formed by the interaction with the suppressor. Fig. 3.11 (d) indicated that the potential in Lev 4 mixture was subsequently maintained to – 178 mV without the deactivation, owing to the strong inhibition layer by interaction between Lev 4 and the suppressor. As shown in Table. 3.2, Lev 4 mixture showed the largest potential difference of –157 mV, and the potential difference in Lev 1, Lev 2, and Lev 3 mixture was almost the same.
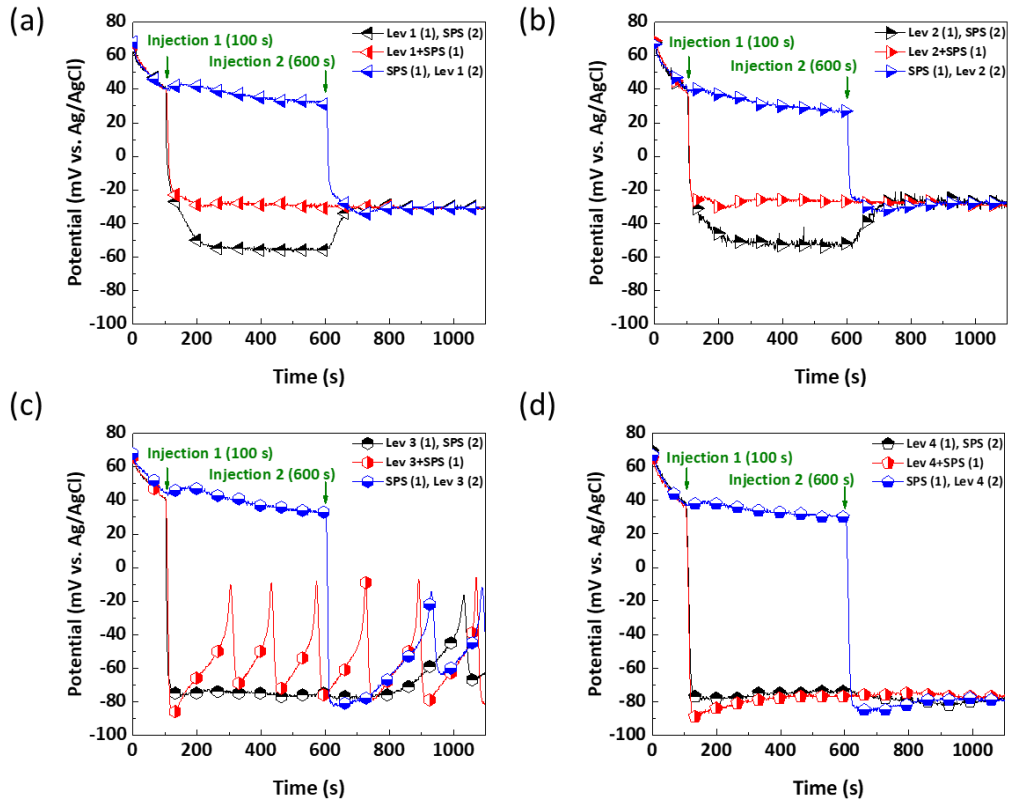
Figure 3.10. Chronopotentiometry (J=15 mA/cm^2) measured at 1000 rpm varying the sequence of 6 μM SPS and 7 μ Lev X (X = (a) 1, (b) 2, (c) 3, and (d) 4) additive injection.
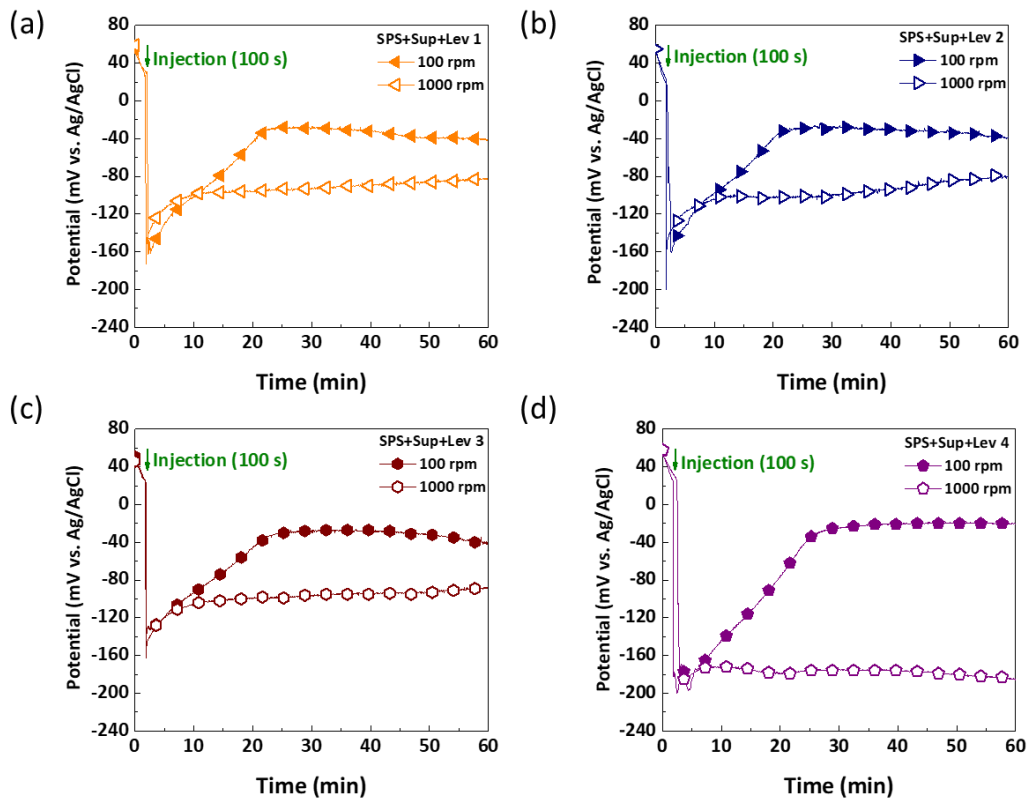
Figure 3.11. Chronopotentiometry (J=15 mA/cm^2) obtained at different rotational speeds in the presence of three–additive mixture: 6 μM SPS, 100 μM PPG–PEG–PPG (Sup) and 7 μM Lev X (X = (a) 1, (b) 2, (c) 3, and (d) 4).

Table. 3.2. Potential Difference Values between 100 and 1000 rpm in Three–additive

Mixture: SPS, PPG–PEG–PPG, and Lev X (X = 1, 2, 3, and 4)

	$V_{100\ rpm}$ (mV)	$V_{1000\ rpm}$ (mV)	ΔV^* (mV)
Lev 1	-35(±5)	-88(±3)	54(±8)
Lev 2	-32(±3)	-91(±7)	59(±10)
Lev 3	-31(±4)	-93(±2)	62(±6)
Lev 4	-21(±2)	-178(±3)	157(±5)

$^*\Delta V = V_{100rpm} - V_{1000rpm}$

3.2.3. Filling performance of microvia with synthesized levelers.

Fig. 3.12 exhibited via filling performance. The potential difference is extended to predict the inhibition difference between top and bottom of via and the filling performance.[48,81] Considering the potential difference in Fig. 3.11, the filling performance would be the best for Lev 4 mixture. As expected, the via filled with Lev 4 mixture formed the fully filled state without voids. The amount of Cu deposited inside the via became noticeably greater with time from 30 to 60 min. On the other hand, other vias were fully unfilled in spite of the bottom–up filling profiles. Through the cross–sectional images, the filling ratio and top thickness of vias were compared quantitatively (Fig. 3.13). The filling ratio was calculated by dividing the area of via deposited with Cu by the total area of via. The top thickness was determined by measuring the thickness of deposited Cu on the top of via excluding the thickness of a Cu seed layer. From Lev 1 to Lev 3 mixture, the filling ratio reached 70, 72, and 89% at 60 min. It is noticeable that the filling ratio in Lev 4 mixture reached 100% at only 50 min with the top thickness of only about 15 μm, whereas the other mixtures obtained the top thickness of about 25 μm. It was remarkable that the sturdy inhibition layer by Lev 4 composed of naphthylmethyl groups contributed to the best filling performance.

In conclusion, four types of levelers containing quaternary ammonium groups varying terminal functional groups were synthesized, and the structure–property relationship of levelers was examined. The inhibition effect of the synthesized levelers was found to increase in order of Lev 1≈ Lev 2 < Lev 3 << Lev 4 based on electrochemical analyses of onset potential, exchange current density, and charge transfer resistance. Lev 4 composed of naphthylmethyl groups, which have a larger aromatic system than benzyl groups of Lev 3, resulted in the strongest inhibition for Cu reduction. In particular, the inhibition layer of Lev 4 was not deactivated by SPS, in contrast to the other levelers, and the inhibition layer complexed with the suppressor was also maintained strongly at 1000 rpm. Therefore, the Lev 4 mixture achieved the highest potential difference of – 157 mV and the superior filling ratio of 100% within 50 min, allowing 15 μm in top thickness of microvias. Based on these results, the naphthylmethyl terminal functional groups are very useful for enhancing the inhibition strength of levelers containing quaternary ammonium groups. This study can be helpful for synthesizing the new levelers for Cu electrodeposition.

	10 min	20 min	30 min	40 min	50 min	60 min
Lev 1						
Lev 2						
Lev 3						
Lev 4						
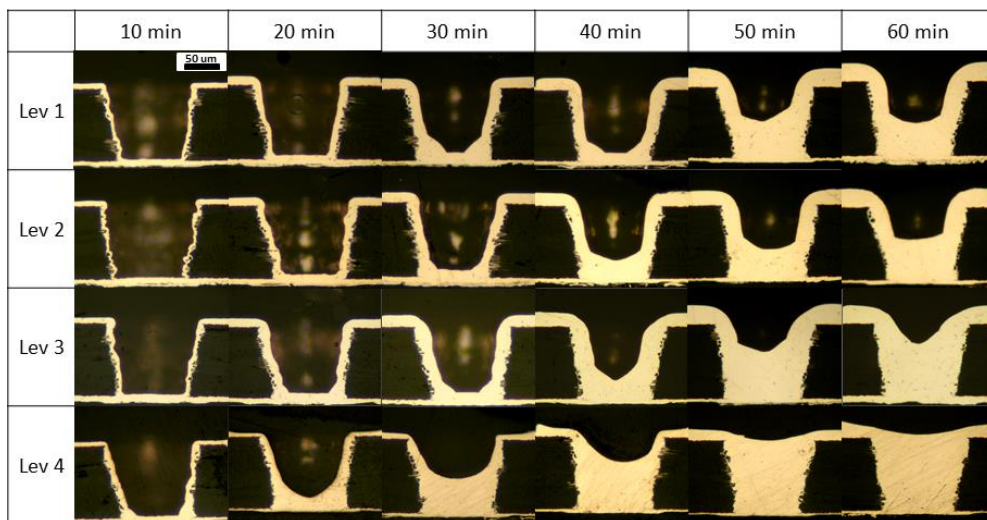
Figure 3.12. Cross–sectional images of microvias electrodeposited varying the deposition times using three–additive mixture: 6 µM SPS, 100 µM PPG–PEG–PPG, and 7 µM Lev X (X = 1, 2, 3, and 4). The current density was –15 mA/cm^2.
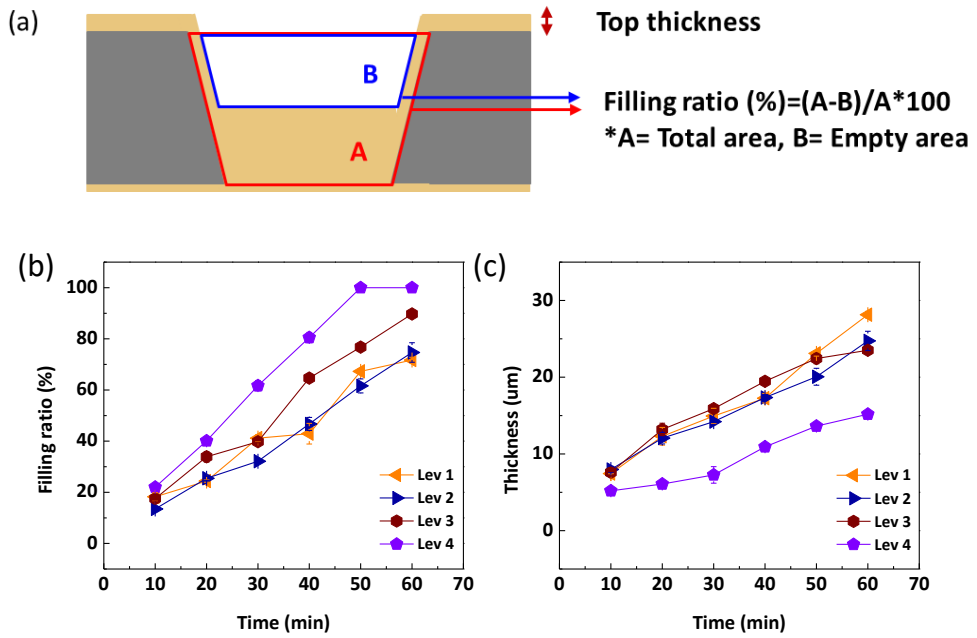
Figure 3.13. (a) Definition of filling ratio and top thickness as filling performance metrics in cross–sectional images of microvias. Plots of the (b) filling ratio and (c) top thickness calculated from filling results in Fig. 3.12.

3.3. Quaternary ammonium groups of levelers

Ammonium groups were directly related to the adsorption of TEG−based levelers because of their positive charge. Although the inhibition strength of leveler was enhanced by modifying the terminal functional groups, the change in ammonium groups expect to improve the adsorption strength of levelers. Therefore, we changed the ammonium groups of levelers composed of allyl groups as the terminal functional groups. Additives were synthesized by naming Lev A–1, Lev A–2 (same structure as Lev 1 in Section 3.2.) and Lev A–3 according to the number of ammonium groups based on Lev 1. The role of additives as the leveler was analyzed through electrochemical analyses and applied to microvia filling process.

3.3.1. Electrochemical effect of ammonium groups

The inhibition effect according to the number of ammonium groups was observed by LSV experiments, as shown in Fig. 3.14. The combinations of additives were various to confirm the interaction between leveler and other additives in two rotating speeds. The onset potential at 1000 rpm in Lev conditions became negatively increasing from Lev

A–1 to Lev A–3 in sequence (5.6, –61.3, and –99.5 mV, respectively). The enhanced inhibition effect was caused by adsorbing more strongly on Cu surface as the ammonium groups that could be adsorbed by their charge interaction increased. When SPS (Acc) was added in Lev condition, Lev A–1 and Lev A–2 indicated weak acceleration effect regardless of rotating speeds. However, in Lev A–3 (Fig. 3.14 (e) and (f)), the current density in the region after the onset potential of Lev A–3 decreased unlike other levelers. It was caused that the interaction between SPS and Lev A–3 formed the synergistic inhibition effect during the desorption of Lev A–3. In the composition of Lev+Sup, Lev weakly affected the inhibition layers that were dominant by the interaction between Sup and Br$^-$ because all plots containing Sup were overlapped according to levelers. However, when SPS was added into the electrolyte composed of Lev+Sup, the current densities showed the acceleration difference that was caused by each levelers.

The interaction between SPS and Lev was analyzed by the injection method in chronopotentiometry to confirm the deactivation of Lev. Fig. 3.15 was obtained by injecting Lev at 100 s and SPS at 600 s in sequence. Lev A–1 showed the constant potential in spite of the addition of SPS and the weakest inhibition strength among them. Weak inhibition effect of Lev A–1 meant that the surface coverage of Lev A–1 at the same concentration was lower than other levelers because it has just one ammonium

groups on the structure of leveler. Lev A–2 was deactivated by SPS, which was equally confirmed in Lev 1 of Fig. 3.10. The potential of Lev A–3 indicated the largest overpotential, −100 mV, that was the best inhibition strength among the synthesized levelers in Section 3.2 and 3.3. In addition, the specific potential shift was obtained by the addition of SPS. The potential moved from –100 to –130 mV in the negative direction immediately after SPS was added. And then, after 60 s, the potential showed a tendency to move in a positive direction again. This results suggested that the interaction between Lev A–3 and SPS initially resulted in the additional inhibition effect and the acceleration effect appeared after a certain period of time.

Microvia filling was examined to confirm the filling performance of Lev A–1, A–2 and A–3. The cross–sectional images of microvia was confirmed in three–additives composition containing the same concentration of Lev, as shown in Fig. 3.16 (a). The deposition amount of Cu inside microvia increased from Lev A–1 to Lev A–3. The thickness of deposited Cu at the bottom of microvia was 17.2, 45.8, and 61.8 μm (Lev A–1 to Lev A–3). Comparing the filling results, Lev A–3 showed a better filling performance, which could be improved by changing the concentration of SPS. When the concentration of SPS changed from 3 to 24 μM with the fixed Sup and Lev A–3, microvias showed the bottom–up filling at 3 μM. Rather, conformal filling images were

obtained as the concentration of SPS increased. These results were analyzed through the

following chronopotentiometry experiments.

In order to interpret the filling results according the concentration of SPS in Lev A–3

compositions, chronopotentiometry experiments were performed like Fig. 3.17. The

potential profiles for SPS compositions were compared under two rotating speed

conditions of 100 and 1000 rpm. At 100 rpm, the potential oscillations were formed in

the range of –20 to –80 mV and the starting time of oscillation was getting faster as the

concentration of SPS increased. It was suggested that the lower supply of Cl^- on the Cu

surface at 100 rpm undermined the inhibition layers of Sup–Cl^- that could be easily

detached by the competitive adsorption of SPS.[22] For the reasons, the adsorbed SPS

induced the repetitive adsorption and desorption of the inhibition layers during the

competitive adsorption with Lev A–3. These potential oscillations were founded in

specific leveler (Lev 3 in Section 3.2) and reported by several papers.[53,75] These

behaviors might be related to the adsorption strength of Lev compared to SPS. At 1000

rpm, the inhibition layers were not maintained strongly at 6, 12, and 24 µM of SPS (Fig.

3.17 (b)~(d)). The potentials at 1000 rpm gradually overlapped with the range of

potential at 100 rpm. These results represented that the inhibition difference between top

and bottom became less and less when the concentration of SPS increased. However, in

Fig. 3.17 (a), the inhibition layers at 1000 rpm were maintained in 3 μM of SPS more than the others, which induced a high potential difference. Although the potential oscillation similarly occurred at 100 rpm in 3 μM of SPS, the concentration of SPS was low to weaken the inhibition layers at 1000 rpm. For the above reasons, microvias can obtain bottom–up filling.
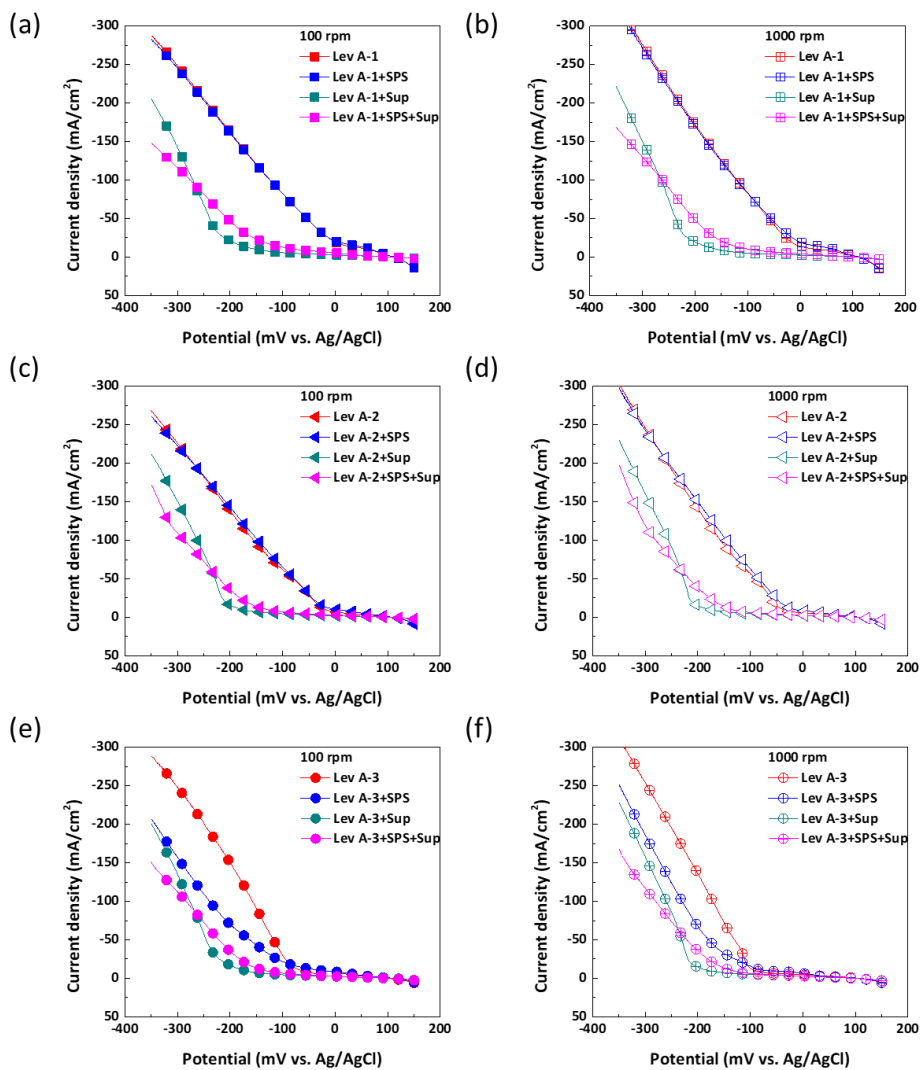
Figure 3.14. LSV curves for Cu reduction with various combinations of additives, with

Lev A–X (X=1 (a), (b), 2 (c), (d), and 3 (e), (f)), Lev A–X and SPS, Lev A–X and PPG–

PEG–PPG (Sup), Lev A–X, Acc, and Sup at the rotating speed of (a), (c), (e) 100 and

(b), (d), (f) 1000 rpm. The concentrations of Lev A–X, SPS, and Sup were 7, 6, and 100

μM, respectively.
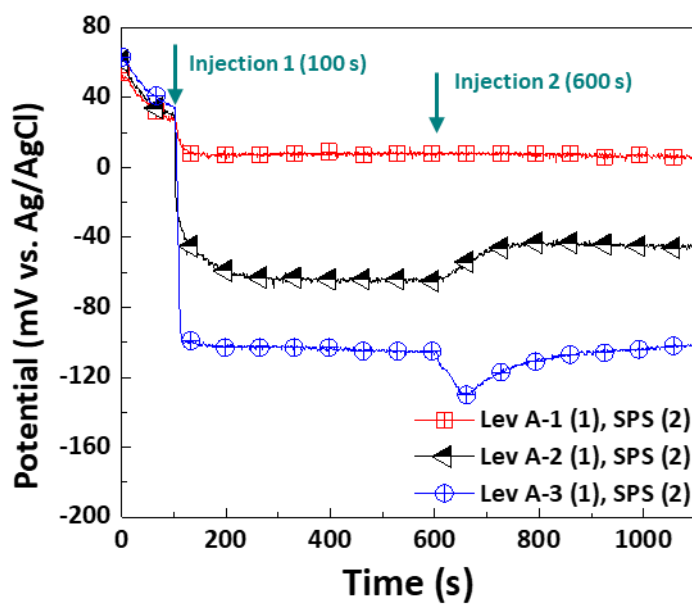
Figure 3.15. Chronopotentiometry measured at 1000 rpm injecting Lev A–X (X=1, 2, and 3) at 100 s and SPS at 600 s in sequence.
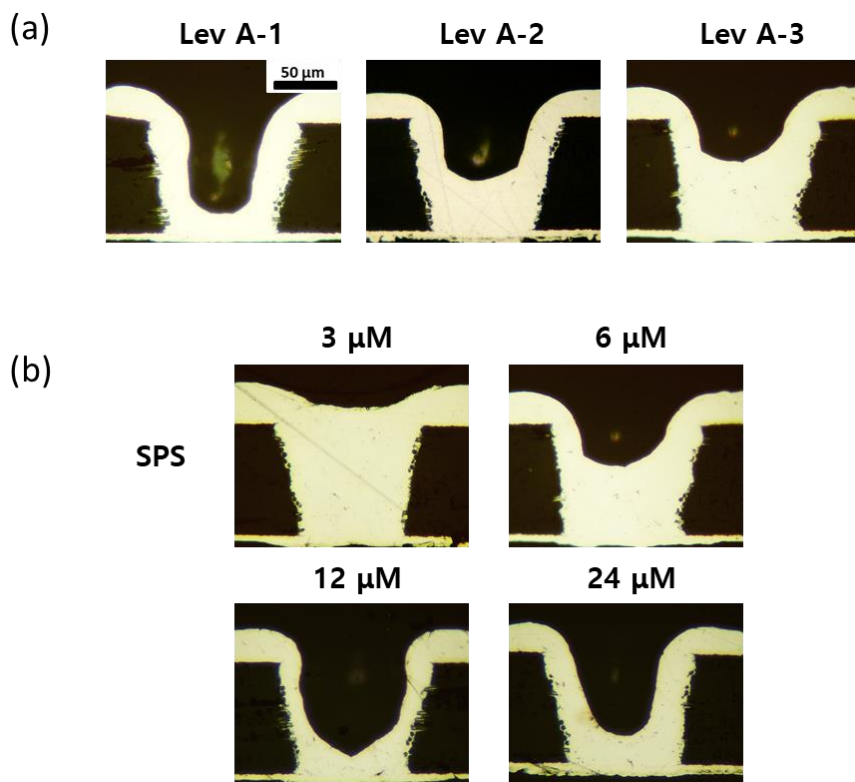
Figure 3.16. Cross–sectional images of microvia deposited by the additives: (a) 6 μM SPS, 100 μM PPG–PEG–PPG and 7 μM Lev A–X (X=1, 2, and 3). (b) The concentrations of SPS were 3, 6, 12, and 24 μM in the same concentration of Lev A–3 and PPG–PEG–PPG. The current density was –15 mA/cm^2; the plating time was 60 min.
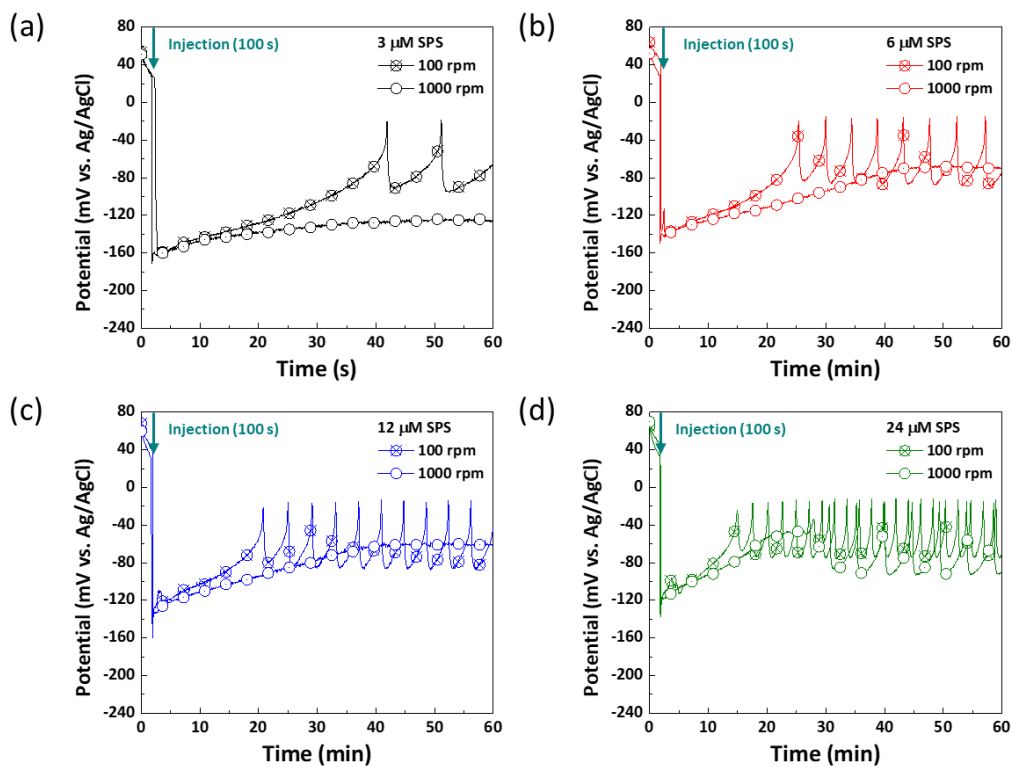
Figure 3.17. Chronopotentiometry observed at two rotating speeds in the presence of three–additives: 3, 6, 12, and 24 µM SPS, 100 µM PPG–PEG–PPG, 7 µM Lev A–3. The current density was –15 mA/cm². All additives were injected at 100 s.

3.3.2. Microvia filling in high current density

The inhibition strength of Lev A–3 was the best among the synthesized levelers in these studies. Although Lev 4 composed of naphthylmethyl as the terminal functional groups was not deactivated by SPS, the inhibition strength of Lev 4 was lower than that of Lev A–3 compared to the deactivation experiments (Fig. 3.10 and Fig. 3.15). Based on these results, Lev A–3 was expected to be applicable to microvia filling in high current density. First, the current density increased from 15 to 30 mA/cm^2 in the additive compositions of Fig. 3.16. The filling time also reduced from 60 to 30 min to adjust the applied charge. All microvias indicated the conformal filling regardless of the concentration of SPS, as shown in Fig. 3.18.

The potentials were measured by applying the current density of 30 mA/cm^2 to understand the filling results in high speed filling, as shown in Fig. 3.19. Comparing the potentials according to the concentration of SPS, the potential difference at 3 µM of SPS gradually was larger from 1200 s in Fig. 3.19 (a), but the difference was not as large as the difference in potential under the condition where microvia filling was successful previously. As the concentration of SPS was higher, the potential difference progressively decreased, and it was nearly zero at 12 µM of SPS (Fig. 3.19 (c)). Since

such a small potential difference was formed, microvias were not fully filled when high current density was applied. The inhibition effect at 1000 rpm was weakened in high current density. It was caused that the inhibition layers dominantly composed of the complexed suppressor layers were strongly detached by more negative overpotential for applying high current density. Therefore, the inhibition effect on the top surface of microvia could not be maintained, which resulted in low inhibition difference between top and bottom of microvias. The configuration of inhibition layers in which the suppression effect was strongly maintained even at high current density needed to be changed. In Fig. 3.20, potential profiles were examined just in SPS and PPG–PEG–PPG condition. Comparing to the result at Fig. 3.19 (a), the potentials were shifted more positive with deposition time regardless of rotating speeds. It meant that polymeric suppressor, PPG–PEG–PPG, can be easily deactivated by SPS and cannot maintain the inhibition layers. For the above reason, it was necessary to conceive inhibition layers expect for PPG–PEG–PPG that occupied a lot of surface coverage on Cu surface by high concentration.

The inhibition layers of Lev A–3 were examined by the injection method to confirm the inhibition strength at high current density except for PPG–PEG–PPG. Lev A–3 was first injected at 100 s, and then SPS was added at 600 s in Fig. 3.20. In 3 μM of SPS, the

potentials showed more negative potential after injecting SPS at 100 and 1000 rpm. As the above results, the interaction between Lev A–3 and SPS was related to the additional negative shift of potential. When the concentration of SPS increased, the time reaching the maximum negative potential gradually increased at all rotating speeds. Therefore, in 6 μM of SPS, the acceleration effect at 100 rpm appeared after the maximum negative potential and exceeded over the inhibition potential of –100 mV in Lev A–3 (Fig. 3.20 (a)) while the potential slowly shifted to positive by 1800s, which was not over –110 mV (Fig. 3.20 (b)). Finally, the inhibition layers at 100 and 1000 rpm were broken by SPS in 12 μM of SPS. Based on these results, high inhibition difference between top and bottom of microvia was formed in the optimum concentration as 6 μM of SPS, which was possible to develop bottom–up filling in high current density.

Varying the concentration of SPS in Lev A–3, the cross–sectional images of microvias were obtained with deposition times, as shown in Fig 3.21. Bottom–up filling was successfully observed when the concentration of SPS changed to 6 μM (Fig. 3.21 (b)). Deposition of Cu proceeded at the corner of bottom with a V–shape until 15 min, but the deposited amount of Cu suddenly was expanded from 22 min 30 s. Although the growth of V–shape initially appeared in 3 μM (Fig. 3.21 (a)), the amount of deposit was insufficient until the complete deposition time. It was caused that low concentration of

SPS induced a weak acceleration effect at the bottom of via. In higher concentration of SPS as Fig. 3.21 (c), the deposit at the corner of bottom was not observed in the initial deposition time. Microvias presented the conformal filling by 30 min. When the specific concentrations of Lev A–3 and SPS were met, it was confirmed that microvias were completely filled in 30 min at 30 mA/cm^2. This deposition time was cut in half from the conventional deposition time.

In this section, the inhibition effect of levelers according the number of ammonium groups were analyzed to apply microvia filling. Lev A–1 and A–2 showed the weak inhibition effect. However, Lev A–3 composed of three–ammonium groups showed the strongest inhibition effect and the specific interaction between Lev A–3 and SPS in the initial deposition time for the competitive adsorption. This interaction enhanced the inhibition effect of Lev A–3 and induced the delayed acceleration effect of SPS. In microvia filing experiments, the conformal filling appeared at all levelers. Among them, when the concentration of SPS decreased to 3 μM in Lev A–3 additives combination, bottom–up filling was obtained because of maintaining the inhibition layers at 1000 rpm. It was tried to perform microvia filling at high current density (30 mA/cm^2). In three–additives composition, all microvias indicated the conformal filling. It was caused that the inhibition layer of PPG–PEG–PPG was easily detached at high current density.

Therefore, the surface coverage of Lev A–3 on Cu surface increased by eliminating Sup, and the inhibition layers was well maintained in spite of the adsorption of SPS. In the optimum concentrations of Lev A–3 and SPS, microvias could form bottom–up filling by applying the current density of 30 mA/cm². The deposition time can reduce from 60 to 30 min. This study can be helpful for developing new levelers in high–speed microvia filling.
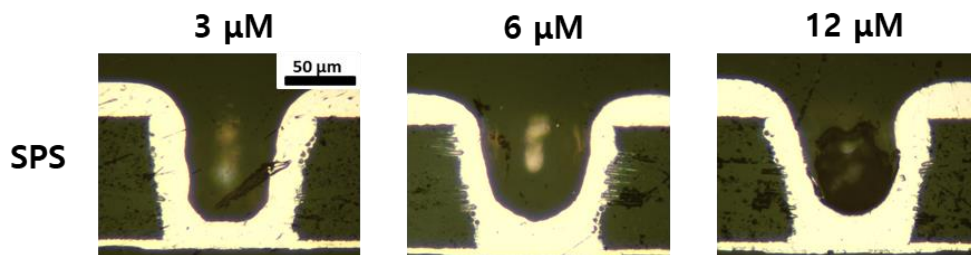
Figure 3.18. Cross–sectional images of microvias by applying the current density of −30 mA/cm^2 in the presence of three–additives: 3, 6, and 12 μM SPS, 100 μM PPG–PEG–PPG, 7 μM Lev A–3. The plating time was 30 min.
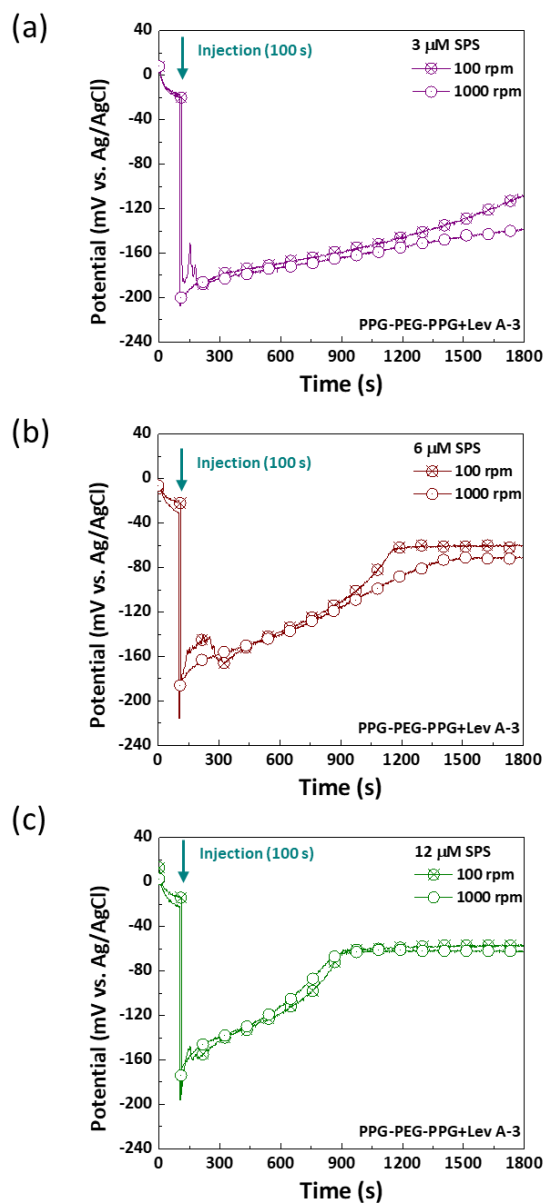
Figure 3.19. Chronopotentiometry observed in high current density of −30 mA/cm^2 in three–additive compositions: 3, 6, and 12 μM SPS, 100 μM PPG–PEG–PPG, 7 μM Lev A–3. All additives were injected at 100 s.
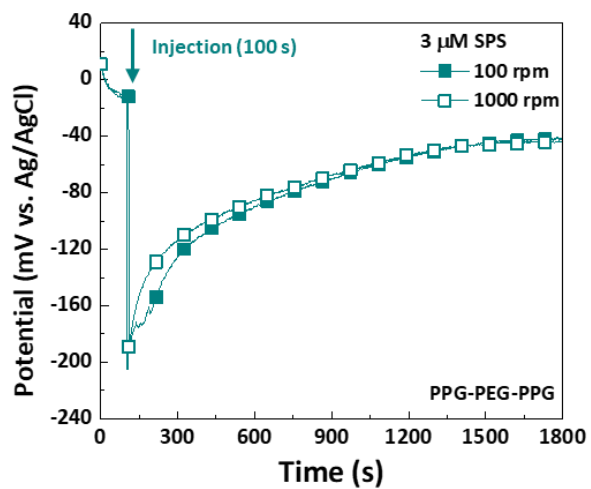
Figure 3.20. Chronopotentiometry observed in high current density of -30 mA/cm^2 in 3

μM SPS and 100 μM PPG–PEG–PPG. All additives were injected at 100 s.
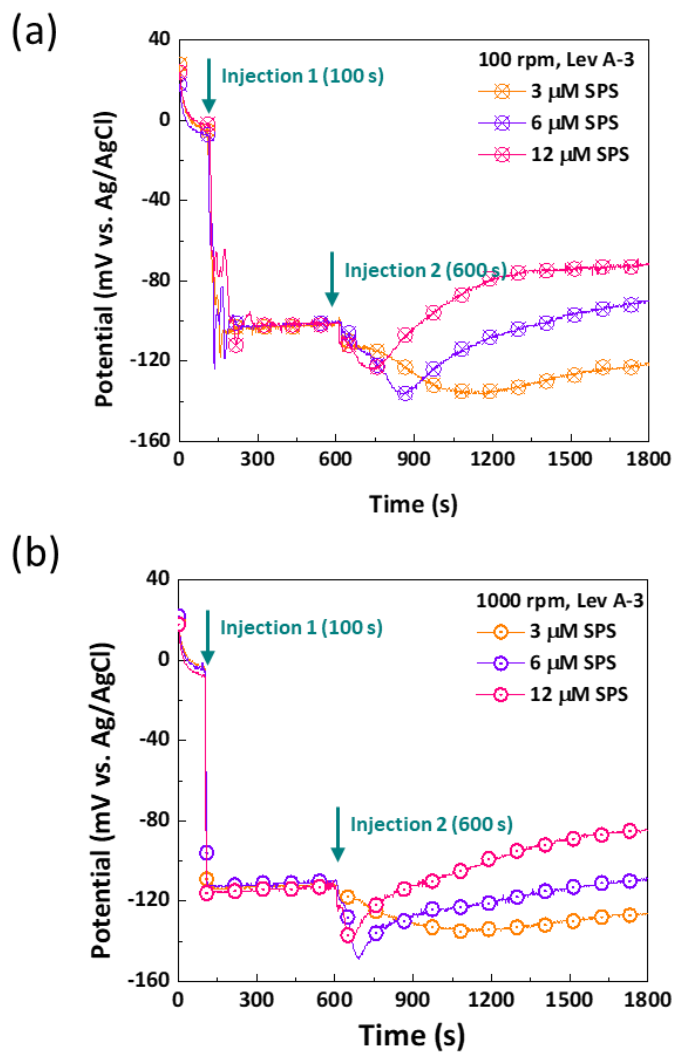
Figure 3.21. Chronopotentiometry at (a) 100 and (b) 1000 rpm according to the concentration of SPS by injecting the additives in sequence: 7 µM Lev A–3 (100 s) and 3, 6, and 12 µM SPS (600 s).
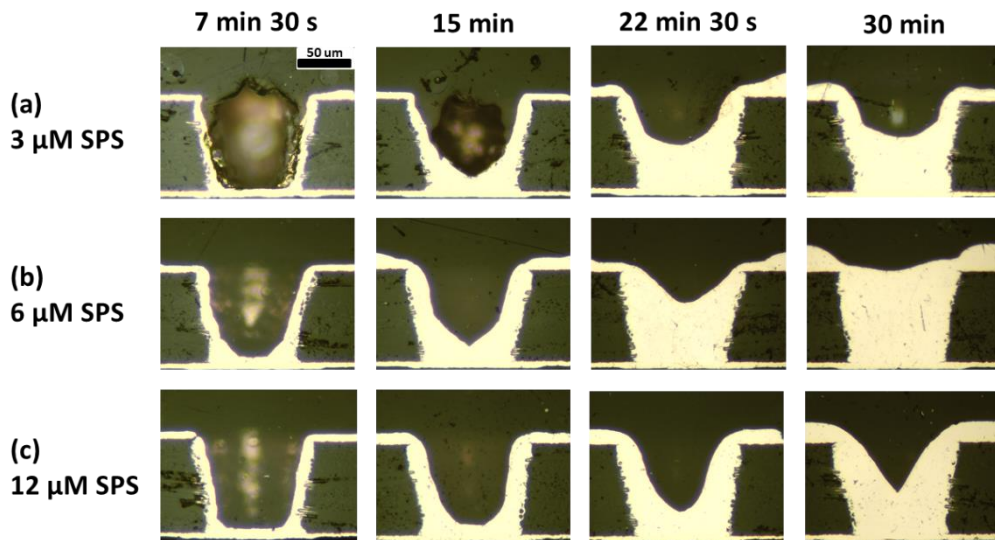
Figure 3.22. Cross–sectional images of microvias according to electrodeposition time in the current density of −30 mA/cm^2. The concentrations of additives were 7 μM Lev A–3 and (a) 3, (b) 6, and (c) 12 μM SPS.

CHAPTER IV

Conclusion

In this study, TEG–based levelers were newly synthesized to improve the inhibition strength by adjusting the structural components of levelers. We first studied the influence of Br^- on the Cu electrodeposition and the interaction of Br^- with other additives. Based on the results, Br^- was adopted as a counter ion of TEG–based levelers. As the method to supplement weaker inhibition effect when using Br^- than I^-, the study was conducted to enhance the inhibition effect through the change of terminal functional groups and the number of ammonium groups.

Halide ions were used as the counter ions in TEG–based levelers. From the reported research in our group, I^- induced the stronger inhibition effect than Br^-, but the deposition efficiency of I^- was lower than that of Br^-. Therefore, the effect of Br^- on the adsorption of PEG and SPS was investigated to apply it as the counter ion. Br^- enhanced the inhibition effect of PEG that was stabilized on the Cu surface. The concentration of SPS and Br^- and the forced convection affected the competitive adsorption between PEG–Br^- inhibition layers and SPS. Therefore, the optimum concentration ratio between SPS and Br^- was dominant for bottom–up filling of microvias. If the addition of Br^- or

SPS was excessive, all of the Cu surfaces could be dominantly covered by PEG–Br⁻ inhibition layers or SPS, which resulted in the conformal filling. In the concentration ratio range (0.2 < [SPS]/[Br⁻] < 0.7), Cu electrodeposition started at the corner of bottom inside microvias and was selectively inhibited outside microvias, leading to Cu bottom–up filling.

Through the study on Br– as the additive, it was sufficient to be effective as the counter ion in TEG–based levelers because Br⁻ could indicate the inhibition effect interacted with other additives. However, the inhibition effect of TEG–based levelers was weakened by displacing I⁻ to Br⁻. Modifying the structures of levelers could compensate the insufficient inhibition. For the reasons, we synthesized TEG–based levelers varying the terminal functional groups. The inhibition strength of synthesized levelers was enhanced in order of Lev 1≈Lev 2 < Lev 3 << Lev 4. Lev 4 composed of naphthylmethyl groups induced the strongest inhibition, which was not deactivated by SPS. In three–additives composition, Lev 4 indicated the highest potential difference of –157 mV. Filling ratio was 100% within 50 min, allowing 15 μm on the top thickness of microvias. Based on the results, naphthylmethyl groups were useful for assisting the inhibition strength of leveler.

Quaternary ammonium groups also could be important for the adsorption of levelers

because of their positive charge. In order to enhance the inhibition effect of levelers, we changed the number of ammonium groups in the structure of Lev 1. Lev A–3 containing three–ammonium groups showed the strongest inhibition effect, which indicated that the interaction between Lev A–3 and SPS induced the synergistic inhibition during the competitive adsorption. In three–additives composition, Lev A–3 showed better performance than other levelers (Lev A–1 and Lev A–2). And the filling performance was improved by changing the concentration of SPS from 6 to 3 μM because of strongly maintaining the inhibition layers at 1000 rpm. When the current density increased in 30 mA/cm^2, microvias showed the conformal filling in the same additive conditions. It was caused that the inhibition layers of PPG–PEG–PPG at 1000 rpm was not maintained due to higher overpotential by the enhanced current density, which resulted in low potential difference. Therefore, the optimum concentration of SPS and Lev A–3 was found to obtain the highest potential difference, which resulted in the high–speed filling in microvia (60 to 30 min).

Overall, the structural components of levelers were considerably related to the inhibition effect of levelers. These studies on Br$^-$, terminal functional groups, and quaternary ammonium groups demonstrated that the inhibition effect of levelers could be enhanced by modification of structure and microvia indicated the improved filling

performance. Especially, these levelers can be useful to obtain specific properties (i.e.

low top thickness and reducing the deposition time) in the electrodeposition industry.

References

1. R. N. Noyce, U.S. Pat., US2981877A (1961).

2. T. K. Gupta, *Microelectron. Reliab.*, **19**, 337–343 (1979).

3. A. K. Sinha, J. A. Cooper, and H. J. Levinstein, *IEEE Electron Device Lett.*, **3**, 90–92 (1982).

4. P. C. Andricacos, C. Uzoh, J. O. Dukovic, J. Horkans, and H. Deligianni, *IBM J. Res. Dev.*, **42**, 567–574 (1998).

5. T. Gupta, *Copper interconnect technology*, p. 423, Springer, Dordrecht ; New York, (2009).

6. B.-H. Huang and S.-H. Chang, *MSSCORPS Co., LTD*. (2018)

7. Takeshi Kobayashi, J. Kawasaki, K. Mihara, and H. Honma, *Electrochimica Acta*, **47**, 85–89 (2001).

8. W.-P. Dow, H.-S. Huang, and Z. Lin, *Electrochem. Solid-State Lett.*, **6**, C134–C136 (2003).

9. W. Dow and H. Chen, *Circuit World*, **30**, 33–36 (2004).

10. D. Carey, *Electronics Design and Manufacturing Symposium,* presentation (2010)

11. W.-P. Dow, M.-Y. Yen, W.-B. Lin, and S.-W. Ho, *J. Electrochem. Soc.*, **152**, C769–C775 (2005).

12. M. Neisser and Kempur Microelectronics, Beijing, China, 101312, *J. Microelectron. Manuf.*, **1**, 1–8 (2018).

13. S.-H. Shin, T.-Y. Kim, J.-H. Park, and S.-J. Suh, *Appl. Sci.*, **8**, 2135 (2018).

14. Y. Zhang, G. Ding, H. Wang, P. Cheng, and R. Liu, *J. Micromechanics Microengineering*, **25**, 045009 (2015).

15. J. Dukovic, S. Ramaswami, S. Pamarthy, R. Yalamanchili, and N. Rajagopalan, in *2010 IEEE International Memory Workshop,*, p. 1–2 (2010).

16. S. Krzewska, *Electrochimica Acta*, **42**, 3531–3540 (1997).

17. Y. Chen, W. He, X. Chem, C. Wang, and Z. Tao., *Electrochimica Acta*, **120**, 293–301 (2014).

18. T. P. Moffat, J. E. Bonevich, W. H. Huber, A. Stanishevsky, D. R. Kelly, G. R. Stafford, and D. Josell, *J. Electrochem. Soc.*, **147**, 4524 (2000).

19. H. Xiao, F. Wang, Y. Wang, H. He, and W. Zhu, *J. Electrochem. Soc.*, **164**, D126–D129 (2017).

20. J.-J. Sun, K. Kondo, T. Okamura, S. Oh, and M, Tomisaka, *J. Electrochem. Soc.*, **150**, G355–G358 (2003).

21. W.-W. Shen and K.-N. Chen, *Nanoscale Res. Lett.*, **12**, 56 (2017).

22. W.-P. Dow, H.-S. Huang, M.-Y. Yen, and H.-C. Huang, *J. Electrochem. Soc.*, **152**, C425–C434 (2005).

23. W.-P. Dow, C.-C. Li, Y,-C. Su, S.-P. Shen, and C.-C, Huang, *Electrochimica Acta*, **54**, 5894–5901 (2009).

24. C. Wang, J. Zhang, P. Yang, and M. An, *Electrochimica Acta*, **92**, 356–364 (2013).

25. L. W. Kong, J. R. Lloyd, K. B. Yeap, E. Zschech, A. Rudack, M. Liehr, and A. Diebold, *J. Appl. Phys.*, **110**, 053502 (2011).

26. A. Nguyen, K. Fealey, P. Reily, G. Pattanaik, and A. Gracias, *J. Microelectron. Electron. Packag.*, **12**, 43–48 (2015).

27. H. P. Zhu, Q. S. Zhu, X. Zhang, C. Z. Liu, and J. J. Wang, *J. Electrochem. Soc.*, **164**, D645–D651 (2017).

28. M. Takeuchi, K. Kondo, H. Kuri, M. Bunya, N. Okamoto, and T. Saito, *J. Electrochem. Soc.*, **159**, D230–D234 (2012).

29. R. Akolkar and U. Landau, *J. Electrochem. Soc.*, **151**, C702–C711 (2004).

30. R. G. Brennan, M. M. Phillips, L.-Y. O. Yang, and T. P. Moffat, *J. Electrochem. Soc.*, **158**, D178–D186 (2011).

31. S. K. Cho, H. C. Kim, M. J. Kim, and J. J. Kim, *J. Electrochem. Soc.*, **163**, D428–D433 (2016).

32. J. Luo, Z. Li, M. Shi, J. Chen, Z. Hao, and J. He, *J. Electrochem. Soc.*, **166**, D104–D112 (2019).

33. S. Zhao, K. Pang, X. Wang, and N. Xiao, *J. Electrochem. Soc.*, **167**, 112502 (2020).

34. P. Broekmann, A. Fluegel. C. Emnet, M. Arnold, and C. Roeger-Goepfert, *Electrochimica Acta*, **56**, 4724–4734 (2011).

35. N. T. M. Hai, T. T. M. Hutnh, A. Fluegel, M. Arnold, and D. Mayer, *Electrochimica Acta*, **70**, 286–295 (2012).

36. J. W. Gallaway and A. C. West, *J. Electrochem. Soc.*, **155**, D632–D639 (2008).

37. Z. V. Feng, X. Li, and A. A. Gewirth, *J. Phys. Chem. B*, **107**, 9415–9423 (2003).

38. D. Stoychev and C. Tsvetanov, *J. Appl. Electrochem.*, **26**, 741–749 (1996).

39. Y. Jin, K. Kondo, Y. Suzuki, T. Matsumoto, and D. P. Barkey, *Electrochem. Solid-State Lett.*, **8**, C6–C8 (2005).

40. M. Kang and A. A. Gewirth, *J. Electrochem. Soc.*, **150**, C426–C434 (2003).

41. M. L. Walker, L. J. Richter, and T. P. Moffat, *J. Electrochem. Soc.*, **152**, C403–C407 (2005).

42. J. J. Kelly and A. C. West, *J. Electrochem. Soc.*, **145**, 3477–3481 (1998).

43. T. P. Moffat, D. Wheeler, S.-K. Kim, and D. Josell, *J. Electrochem. Soc.*, **153**, C127–C132 (2006).

44. T. P. Moffat, D. Wheeler, W. H. Huber, and D. Josell, *Electrochem. Solid State Lett.*, **4**, C26 (2001).

45. T. P. Moffat, D. Wheeler, M. D. Edelstein, and D. Josell, *IBM J. Res. Dev.*, **49**, 19–36 (2005).

46. J. W. Gallaway, M. J. Willey, and A. C. West, *J. Electrochem. Soc.*, **156**, D287 (2009).

47. F. Wang, P. Zeng, Y. Wang, X. Ren, H. Xiao, and W. Zhu, *Microelectron. Eng.*, **180**, 30–34 (2017).

48. W.-P. Dow and C.-W. Liu, *J. Electrochem. Soc.*, **153**, C190–C194 (2006).

49. W.-P. Dow, C.-C. Li, M.-W. Lin, G.-W. Su, and C.-C. Huang, *J. Electrochem. Soc.*, **156**, D314–D320 (2009).

50. J. J. Kelly, C. Tian, and A. C. West, *J. Electrochem. Soc.*, **146**, 2540–2545 (1999).

51. M. J. Kim, H. C. Kim, and J. J. Kim, *J. Electrochem. Soc.*, **163**, D434–D441 (2016).

52. Y.-B. Li, W. Wang, and Y.-L. Li, *J. Electrochem. Soc.*, **156**, D119–D124 (2009).

53. W. Wang, H. Hua, L. Yin, and Y. He, *J. Electrochem. Soc.*, **161**, D651–D656 (2014).

54. J. Xu, B. Chen, J. Lv, D. Chang, and D. Niu, *Dyes Pigments*, **170**, 107559 (2019).

55. M. Takeuchi, Y. Yamada, M. Bunya, S. Okada, N. Okamoto, T. Saito, and K. Kondo, *J. Electrochem. Soc.*, **160**, D3110–D3115 (2013).

56. Q. Zhang, X. Yu, Y. Hua, and W. Xue, *J. Appl. Electrochem.*, **45**, 79–86 (2015).

57. J. Lv, X. Zhao, X. Jie, J. Li, and X. Wei, *ChemElectroChem*, **6**, 3254–3263 (2019).

58. A. Wang, B. Chen, L. Fang, J. Yu, and L. Wang, *Electrochimica Acta*, **108**, 698–706 (2013).

59. T. Lu, F. Wang, and Y. He, *J. Electrochem. Soc.*, **163**, D663–D671 (2016).

60. J. J. Hatch, M. J. Willey, and A. A. Gewirth, *J. Electrochem. Soc.*, **158**, D323 (2011).

61. M. J. Kim, Y. Seo, J. H. Oh, Y. Lee, H. C. Kim, Y. G. Kim, and J. J. Kim, *J. Electrochem. Soc.*, **163**, D185–D187 (2016).

62. K. Kondo, Y. Yamada, and M. Yokoi, *J. Electrochem. Soc.*, **162**, D397–D400 (2015).

63. S. Huemann, N. T. Minh Hai, P. Broekmann, K. Wandelt, H. Zajonz, H. Dosch, and F. Renner, *J. Phys. Chem. B*, **110**, 24955–24963 (2006).

64. T. M. T. Huynh, F. Weiss, N. T. M. Hai, W. Reckien, and T. Bredow, *Electrochimica Acta*, **89**, 537–548 (2013).

65. M. Sung, Y. Yoon, J. Hong, M. J. Kim, and J. J. Kim, *J. Electrochem. Soc.*, **166**, D546 (2019).

66. R. C. Alkire and D. M. Kolb, Eds., *Electrochemical surface modification: thin films, functionalization and characterization*, p. 107-189, Wiley-VCH-Verl, Weinheim, (2008).

67. M. Hayase, M. Taketani, T. Hatsuzawa, and K. Hayabusa, *Electrochem. Solid State Lett.*, **6**, C92 (2003).

68. K. Doblhofer, S. Wasle, D. M. Soares, K. G. Weil, G. Weinberg, and G. Ertl, *Z. Für Phys. Chem.*, **217**, 479–492 (2003).

69. G.-K. Liu, S. Zou, D. Josell, L. J. Richter, and T. P. Moffat, *J. Phys. Chem. C*, **122**, 21933–21951 (2018).

70. R. Mroczka and A. Słodkowska, *Electrochimica Acta*, **339**, 135931 (2020).

71. D. Barkey, R. Chang, D. Liu, and J. Chen, *J. Electrochem. Soc.*, **161**, D97 (2013).

72. P.-F. Chan and W.-P. Dow, *J. Electrochem. Soc.*, **166**, D891–D897 (2019).

73. Q. Huang, B. C. Baker-O'Neal, C. Parks, M. Hopstaken, and A. Fluegel, *J. Electrochem. Soc.*, **159**, D526–D531 (2012).

74. N. T. M. Hai, J. Odermatt, V. Grimaudo, K.W. Kramer, A. Fluegel., *J. Phys. Chem. C*, **116**, 6913–6924 (2012).

75. V. Grimaudo, P. Moreno-Garcia, A. Riedo, A. C. Lopez, and M. Tulej, *J. Electrochem. Soc.*, **166**, D3190 (2018).

76. D. Josell, T. P. Moffat, and D. Wheeler, *J. Electrochem. Soc.*, **154**, D208 (2007).

77. M. Schlesinger and M. Paunovic, *Modern Electroplating*, **5th**, p5, John Wiley & Sons, New york (2010)_.

78. L. Bartels, *Nat. Chem.*, **2**, 87–95 (2010).

79. N. Atodiresei, V. Caciuc, P. Lazić, and S. Blügel, *Phys. Rev. Lett.*, **102**, 136809 (2009).

80. Y. E. Jo, D. Y. Yu, and S. K. Cho, *J. Appl. Electrochem.*, **50**, 245–253 (2020).

81. W.-P. Dow, M.-Y. Yen, C.-W. Chou, C.-W. Liu, W.-H. Yang, and C.-H. Chen, *Electrochem. Solid-State Lett.*, **9**, C134–C137 (2006).

국문 초록

구리 전해도금은 전자기기 산업에서 인쇄 회로 기판과 집적 회로에서의 배선을 위한 기술로서 공통적으로 이용되었다. 배선의 높은 신뢰성을 위해서는 다양한 첨가제들을 사용하면서 바닥 차오름을 형성하여야 한다. 이러한 첨가제들 중에서 평탄제는 마이크로비아의 바닥 차오름에 중요한 역할을 하며, 더 나은 채움 특성을 위해 평탄제의 개발은 필수적이다. 억제효과를 상승시키기 위해서 평탄제의 구조 변화는 필요하다, 그러나 구조에 따른 평탄제의 억제 거동에 대한 연구는 아직 불충분한 상태이다. 본 연구에서는 억제 세기를 상승시키기 위해 트라이에틸렌 글라이콜 기반의 평탄제들의 말단 작용기 그룹 그리고 4가 암모늄 그룹들과 같은 구조들을 조절하는 것과 브로마이드 이온과 가속제 사이의 상호작용에 대한 연구를 진행하였다.

첫번째 연구는 중합체의 억제제와 가속제의 흡착에 대한 브로마이드 이온들의 영향에 대해 살폈다. 비록 브로마이드 이온들은 반대 이온들로 사용되었지만, 무기 첨가제로서 적용을 할 수 있다. 브로마이드 이온들은 구리 표면에서 억제 효과를 보이고 억제제의 억제 층이 안정화 된다. 가속제와의 경쟁 흡착은 가속제와 브로마이드 이온들의 농도와 강제 대류에 좌우된다. 첨가제의 농도비가 특정 범위(0.2 < [SPS]/[Br] < 0.7) 안에서,

마이크로비아의 바닥 모서리에서 구리를 도금하고 위 표면을 억제함으로써 마이크로비아는 바닥 차오름을 형성 할 수 있다. 만약 이 농도 범위에서 벗어난다면, 등각 채움이 형성 된다.

브로마이드 이온은 첨가제들과 상호작용으로 형성된 억제 효과의 이유로 TEG 기반의 평탄제에서 반대이온으로서 선택되었다. 평탄제들은 부족한 억제를 보충하기 위해 구조를 수정할 필요성이 있으며 그 이유로는 아이오다이드 이온에서 브로마이드 이온으로 대체가 평탄제들의 억제 효과를 감소시키기 때문이다. 평탄제들의 억제 특성을 향상시키기 위해서, 말단 작용기들(알릴기, 프로필기, 벤질기, 그리고 나프틸메틸기)을 변화시키면서 TEG 기반의 평탄제들을 합성하였다. 모든 평탄제들에서, 나프틸메틸기가 포함된 평탄제가 가장 억제 효과가 크고 가속제에 의한 비활성화가 나타나지 않음을 보였다. 마이크로비아 채움에서, 평탄제를 포함한 세개의 첨가제들을 사용함으로써 채움 비율은 100%가 50분 안에 도달하였고 마이크로비아의 윗 부분 두께는 15 μm이었다. 결과적으로 나프틸메틸 작용기가 평탄제의 억제 세기를 향상 시키기 위해서 유리한 조건이었다.

게다가, 제4 암모늄 작용기는 양전하 때문에 평탄제의 흡착에 관련될 수 있다. 우리는 제4 암모늄 작용기의 수에 따른 평탄제들의 억제 효과를 또한

조사하였다. 세개의 암모늄 작용기를 포함한 평탄제는 이 연구에서 합성한 첨가제들 중에서 가장 강한 억제효과를 이끌었다. 그리고 평탄제와 가속제 사이에서의 상호작용이 경쟁 흡착 동안 상승적인 억제를 만들어내는 것을 보였다. 첨가제들의 특정 농도에서 세개의 암모늄 작용기가 있는 평탄제를 사용함으로써 바닥 차오름이 형성 되었고, 또한 전류 밀도를 15에서 30 mA/cm^2 향상 시킴으로써 바닥 차오름을 얻을 수 있었다. 놀랍게도, 구리 도금 속도는 60분에서 30분으로 줄었다.

이러한 연구들은 구리 전해도금 산업에서 새로운 평탄제를 분석하고 제안하는데 있어 도움이 될 수 있다.

Appendix I

Evaluation of convection-dependent adsorption behavior of quaternary ammonium-based leveler

Convection dependent adsorption behavior of levelers was important to perform bottom-up filling of microvias. In this study, the synthesized leveler was examined by electrochemical analyses such as LSV and Koutecký–Levich plot.

1. Introduction

Copper electroplating is used for the metallization in printed circuit boards (PCBs) and integrated circuits (ICs) in the electronics industry. Because microvia or through-holes are essential components for the multilayer structure of devices,[1,2] completely void- and seam-less filling, so called "superfilling" or "bottom-up filling," ensures the reliability and stability of the interconnects.[3–6] Superfilling is generally achieved by adding a combination of several additives, such as an accelerator, a suppressor, and a leveler, to a copper electroplating solution: bis(3-sulfopropyl) disulfide (SPS) or 3-

mercapto-1-propaesulfonate (MPS) as the accelerator,[7,8] polyethylene glycol (PEG), polypropylene glycol (PPG), or their copolymer as the suppressor,[1,9] and Janus Green B (JGB) or Diazine Black (DB) as the leveler.[10–12] Void-free filling of microvias is associated with the variation of the local deposition rate, where the leveler would selectively inhibit the Cu deposition reaction on the protrusions on the rough surface to make a flat surface.[13,14]

A number of levelers have quaternary ammonium groups in their molecular structures,[15–18] which plays a key role in the adsorption and inhibition function of the levelers. The electrostatic attraction between the positive charge on nitrogen atoms and the negatively charged Cu surface leads to the non-specific adsorption of the leveler on Cu surface and the physical inhibition of Cu deposition.[19,20] Moreover, quaternary ammonium-based leveler was reported to be electrochemically reducible, which would decrease the faradaic efficiency for Cu electroplating.[21] The adsorption phenomenon depends on the electrode geometry and the potential, thus resulting in local variation of the inhibition function of the leveler. The other important characteristic of the leveler in association with the filling performance is its convection-dependent adsorption (CDA); as the forced convection of the electrolyte becomes more vigorous, the adsorption and inhibition functions of the leveler become more severe. Typically, the electrolyte in the

vicinity of the bottom of the microvia is quiescent compared to that at the top, and thus CDA behavior enhances the deposition rate at the bottom.[22,23] The CDA behavior of various levelers and its interaction with halide ions[24,25] and other additives[6,26] have been studied. Usually, the potential difference between 100 rpm and 1000 rpm for galvanostatic Cu electrodeposition can be considered an indicator of filling performance.[6,27]

In this study, we synthesized the leveler that had a hexaethylene glycol structure with quaternary ammonium functional groups. Polyether bonded to dialkylamine or quaternary amine has been proposed as an effective suppressor,[28] and previously we synthesized a triethylene glycol-based leveler and successfully applied it to filling in through silicon vias.[24] The quaternary ammonium-based leveler presented in this study was investigated electrochemically and applied to microvia filling. In addition, its CDA behavior was characterized with a rotating disk electrode (RDE) and a Koutecký–Levich plot.

2. Experimental

The quaternary ammonium-based leveler was synthesized as shown in Scheme 1.

Hexaethylene glycol diallyl ether (**1**) was obtained from the O-allylation reaction of ethylene glycol by the allyl bromide and tetrabutylammonium iodide (TBAI). The epoxidation reaction of **1** with meta-chloroperoxybenzoic acid (mCPBA) resulted in the change from an allyl group to an epoxide ring group, forming compound **2**. Treatment of **2** with N,N-dimethylamine opened the epoxide ring and then we added dimethylamine groups to form compound **3.** The quaternary ammonium-based leveler was produced from the N-allylation reaction of **3** with allyl bromide. The structure of the synthesized leveler was confirmed by ^{1}H, ^{13}C nuclear magnetic resonance (NMR) spectra and high resolution mass spectroscopy (HRMS) data.

A PCB substrate (Samsung Electro-Mechanics Co. Ltd.) was prepared as the cathode, with dimensions of 2.1 cm × 2.2 cm. The dimensions of the microvia formed by laser drilling on the PCB substrate were 130 μm in width at the top, 100 μm at the bottom, and 100 μm in depth. Each substrate had about 1750 microvias and the distance between microvias was 300 μm in average. Prior to the formation of a seed layer, the substrate went through desmear process to remove the laminate fragments and to enhance the adhesion between a Cu seed layer and a substrate, followed by conditioning and acid etching. A Cu seed layer (3 μm) was formed on the PCB substrate by electroless deposition method. The insoluble anode (IrO$_2$/Ti) covered by a proton-conducting

membrane was used as the anode. The plating solution was composed of 0.92 M

CuSO$_4$•5H$_2$O (99+% purity, SEO AN CHEM TEC), 0.43 M H$_2$SO$_4$ (95% purity,

DAEJUNG), and 0.82 mM HCl (35% purity, DAEJUNG). 6 μM SPS (Raschig GmbH,

Germany), a 100 μM PPG-PEG-PPG copolymer (M$_w$ = 2000, Sigma Aldrich), and a 7

μM synthesized leveler were added to the plating solution contained in a polypropylene

bath (2 L). The electrolyte was ejected from a nozzle installed in the bath to the substrate,

where the nozzle pressure was maintained at 0.5 kgf/cm^2. The distance between a nozzle

and a PCB substrate was 5 cm. The temperature of the plating solution was maintained

at 25°C. The current density for galvanostatic copper electroplating was 15 mA/cm^2 and

the plating time was 60 min. After copper electroplating, the substrate was sectioned and

its cross-section was observed with an optical microscope (ICS-306B, SOMETECH).

About 30 microvias on each substrate were inspected in order to examine the filling

profile of Cu in microvia.

   Electrochemical analyses were performed to investigate the inhibition effect and CDA

behavior of the synthesized leveler. The analyses were carried out with a three-electrode

system containing a Cu RDE (geometric area = 0.07 cm^2) as the working electrode, Cu

wire as the counter electrode, and Ag/AgCl (KCl sat.) as the reference electrode. The Cu

RDE was ground with 2000 grit sand paper and washed with deionized water. Linear

sweep voltammetry (LSV) was performed by sweeping the potential from 150 mV (vs. Ag/AgCl) to −350 mV at a scan rate of 10 mV/s. Chronoamperometry was performed at the potentials of 0, −50, −100, and −150 mV (vs. Ag/AgCl) for 120 s. All electrochemical measurements were carried out with a PAR 263 A Potentiostat (EG&G Princeton Applied Research Corporation).

3. Results and Discussion

Cu was electroplated into the microvia with the combination of accelerator–suppressor–leveler, and its time-evolving deposit profiles are shown in Fig. 1. When the synthesized leveler was added into the plating electrolyte, bottom-up filling was clearly observed in the microvia as compared to the leveler-free condition. The higher deposition rate at the bottom as compared to at the top indicates that the synthesized leveler suppressed the growth of Cu on the top of the microvia. It is presumed that the inhibition power, which varied with the position on the microvia, would be associated with electrolyte convection.

The inhibition effect of the leveler on Cu electroplating was examined via LSV analyses on Cu RDE, where rotating speeds of 100 and 1000 rpm were adopted in order

to replicate the conditions of the electrolyte convection on the bottom and top of the microvia, respectively, and the results are presented in Fig. 2. When the leveler was added into the electrolyte, Cu deposition was effectively suppressed for the overall potential range (Fig. 2a). The inhibition effect of the leveler was less severe than that of the suppressor, which might be due to the difference in the amount of addition. The inhibition effect of the leveler was also found on the combination with suppressor–accelerator (Fig. 2b). In principle, the high rotating speed of the RDE enhances the mass transfer of cupric ions to the electrode surface, leading to a high current density. However, the effect is not very significant at low overpotentials where the current density depends on the charge-transfer rate rather than on the mass-transfer rate. Actually, in all LSV measurements without the leveler, the curves for 100 and 1000 rpm were almost identical until the potential reached -200 mV (vs. Ag/AgCl); subsequently, the rotation with 1000 rpm exhibited higher current beyond -200 mV. (Figs. 2a and b). However, with the addition of the leveler, the current at 1000 rpm was lower than that at 100 rpm in the potential range from 50 to -200 mV, and it manifested CDA behavior.

The CDA behavior of the leveler was investigated via chronoamperometry. Because the electrochemical reduction of Cu^{2+} to Cu is not very reversible, the current for the backward reaction (from Cu^0 to Cu^{2+}) can be ignored, and therefore, the current in the

presence (i_{Lev}) and absence (i_{no}) of the leveler can be expressed as follows:

$$i_{Lev} = nFAC_{Cu^{2+}}(t)k_{Lev}(E)\theta(t) + nFAC_{Cu^{2+}}(t)k_{no}(E)\big(1 - \theta(t)\big) \quad (1)$$

$$i_{no} = nFAC_{Cu^{2+}}(t)k_{no}(E) \quad (2)$$

where n is the number of electrons involved in the reaction, A is the electrode area, $C_{Cu^{2+}}$ (t) is the concentration of Cu^{2+} at the electrode surface, and k is the rate constant with and without the leveler. θ is the fractional coverage of the leveler [$\theta(t) = \Gamma(t)/\Gamma_s$, where Γ and Γ_s are the surface excess of the leveler at time t and at saturation, respectively], assuming that the adsorption type of the leveler is specific, which is consistent with the observation by Hai et al.[21] In the chronoamperometric measurement on the RDE, the current varied with time because of the change in Cu^{2+} concentration and the coverage of the leveler. A steady-state value for the current indicates that the diffusion boundary layer of Cu^{2+} is fully developed and that the coverage of leveler is almost equal to the equilibrium coverage, $\theta_{eq} = \Gamma_{eq}/\Gamma_s$, where Γ_{eq} is surface excess of leveler at equilibrium. Herein, we define

$$i_{diff} = \frac{i_{no} - i_{Lev}}{i_{no}} \quad (3)$$

as the extent of the inhibition effect, which is a function of the concentration of Cu^{2+} and the coverage of the leveler, both of which change with time. Especially, at 0 to -100 mV (vs. Ag/AgCl), the current value was less than 10% of the limiting current density (0.19–

0.74% at 0 mV, 0.43–1.60% at −50 mV, and 1.79–7.29% at −100 mV in the 100–1000

rpm range), whereby the concentration of Cu^{2+} at the RDE surface is almost equal to the

bulk concentration (0.92 M) overall. Then, insertion of Eqs. (1) and (2) into Eq. (3) yields,

$$i_{diff} \approx [k_{no}(E) - k_{Lev}(E)]\theta(t)/k_{no}(E) \quad (4)$$

Because the rate constant is time-independent, i_{diff} manifested the change in the

coverage of the leveler according to the time, which corresponds with the adsorption rate.

Figure 3 shows the plots of i_{diff} against time with the leveler at the potentials where the

CDA behavior was observed in the LSV analyses (0 to −150 mV vs. Ag/AgCl). The

results from the same analyses with the suppressor are also presented in Fig. 3 for

comparison. The suppressor exhibits relative large i_{diff} values as compared to the leveler,

which indicates that the extent of the inhibition effect of the suppressor was larger than

that of the leveler over all potential ranges, which is consistent with the weaker inhibition

effect of the leveler as compared to that of the suppressor in the LSV analyses. The i_{diff}

value for the suppressor did not vary much with time, which indicates the rapid saturation

of its coverage, whereas i_{diff} for the leveler gradually climbed, which indicates the

gradual increase in the surface coverage of the leveler. In addition, i_{diff} for the leveler

varied significantly with the applied potential, indicating that k_{Lev} increased with

increasing applied potential, whereas k_{Sup} was almost constant. Moreover, i_{diff} for the

leveler increased faster with the higher rotating speed, which would correspond to the CDA behavior of the leveler. The adsorption rate would be governed by the rate of adsorption reaction (adsorption reaction model) or by the rate of the mass transfer of the adsorbate (adsorption diffusion model),[29] whereby the CDA behavior might be interpreted in terms of the adsorption diffusion model. For a linearized specific adsorption isotherm (low concentration of the leveler) under a semi-infinite linear diffusion of adsorbate, the coverage of leveler adsorbed at time t is[30]

$$\theta(t) = \frac{\Gamma(t)}{\Gamma_s} = \theta_{eq} \ [1 - \exp(-D_{Lev}t/\delta K\Gamma_s)] \tag{5}$$

where D_{Lev} is a diffusion coefficient of the leveler, δ is the diffusion boundary layer thickness for the leveler, and K is an adsorption equilibrium constant. Because δ is a function of the rotating speed of the RDE, it would contribute to the convection-dependency of the adsorption process; at higher rotating speeds, θ increased more abruptly, which is consistent with the behavior of i_{diff} for the leveler in Fig. 3. According to Eq. (5), the coverage of the leveler would eventually reach same θ_{eq} at all rotating speeds, whereby the difference in the inhibition effect of the leveler according to the convection would gradually vanish during electroplating. However, i_{diff} for the leveler did not converge upon same value, as shown in Fig. 3. After 100 s, i_{diff} reached almost steady-state values ($i_{diff,ss}$), which are plotted against the rotating speed in Fig. 3e.

Although $i_{diff,ss}$ for the leveler was expected to be independent of the rotating speed according to Eqs. (4) and (5), it increased with increasing rotating speed and became more evident with the high overpotential (Fig. 3e). However, $i_{diff,ss}$ for the suppressor was almost constant over all rotating speeds and overpotentials (Fig. 3f). Actually, the adsorption process can be disturbed by the continuous generation of a freshly deposited Cu surface, and thus $i_{diff,ss}$ (or θ_{eq}) for the leveler would vary with rotating speed. Therefore, the adsorption model should be modified with the reaction rate of adsorption and desorption, which will be considered in our future study.

The CDA behavior of the leveler according to the rotating speed is also found in a Koutecký–Levich plot. For a totally irreversible electron-transfer reaction, the Koutecký–Levich relation can be depicted as follows:

$$\frac{1}{i} = \frac{1}{i_k} + \frac{1}{0.62nFAD_{Cu^{2+}}^{2/3}\omega^{1/2}v^{-1/6}C_{Cu^{2+}}^*} \qquad (6)$$

$$i_k = nFAk(E)C_{Cu^{2+}}^* \qquad (7)$$

where ω is the rotating speed, v is the kinematic viscosity of the electrolyte, D_{Cu2+} is the diffusion coefficient of Cu^{2+}, and C^*_{Cu2+} is the bulk concentration of Cu^{2+} in the electrolyte. The y-intercept of a straight line extrapolated to $\omega^{1/2} = 0$ in the plot of $1/i$ vs. $1/\omega^{1/2}$ gives $1/i_k$, whereby θ_{eq} and k_{Lev} (E) could be obtained by Eqs. (4) and (6). The Koutecký–Levich plots for Cu electrodeposition with and without the leveler are

presented in Fig. 4. In the plot for the no-additive condition (Fig. 4a), the slope

$[1/(0.62nFAD^{2/3} \upsilon^{-1/6}C^*_{Cu2+})]$ of the linear line was 0.194 mA^{-1}·s$^{-1/2}$ at 0 mV, and it did

not vary much with the overpotential. This value was close to the theoretical value (0.206

mA^{-1}·s$^{-1/2}$, A = 0.07 cm^2, C = 0.92 M, D = 5 × 10^{-6} cm^2/s,[31] υ = 0.01 cm^2/s). However,

the plot for the leveler showed a negative slope (Fig. 4b), which is consistent with the

chronoamperometric results: a lower current flow at the higher rotating speed. Although

k_{Lev} (E) could not be estimated because of the negative slope, the CDA behavior of the

leveler was clearly shown with the Koutecký–Levich plots.

As the inhibition effect of hexaethylene glycol is almost negligible,[32] the inhibition

effect of the leveler would be originated from cationic nitrogen groups in its molecular

structure and it might be also associated with its convection-dependent adsorption

behavior. Our further research will focus on unveiling the relationship between the

functional group of the leveler and its convection-dependent adsorption behavior.
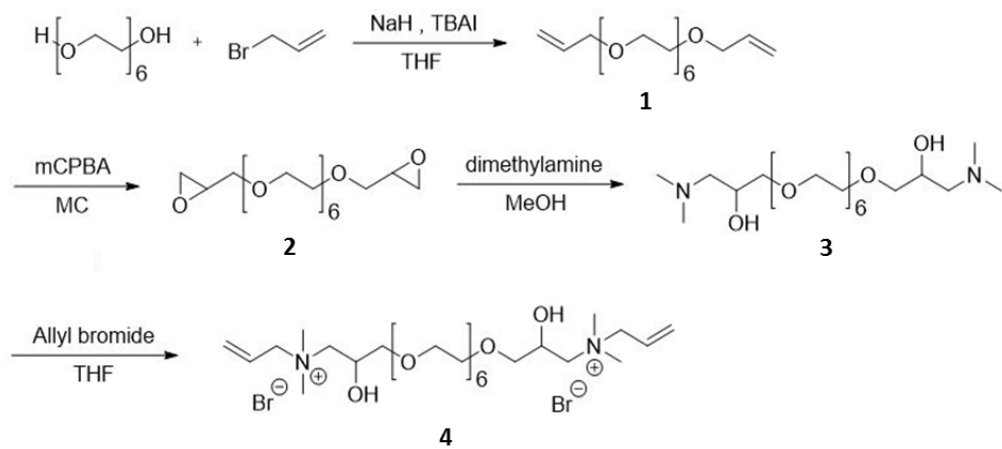
Scheme 1. Synthetic route for a quaternary ammonium-based synthesized leveler with

hexaethylene glycol and allyl functional groups.
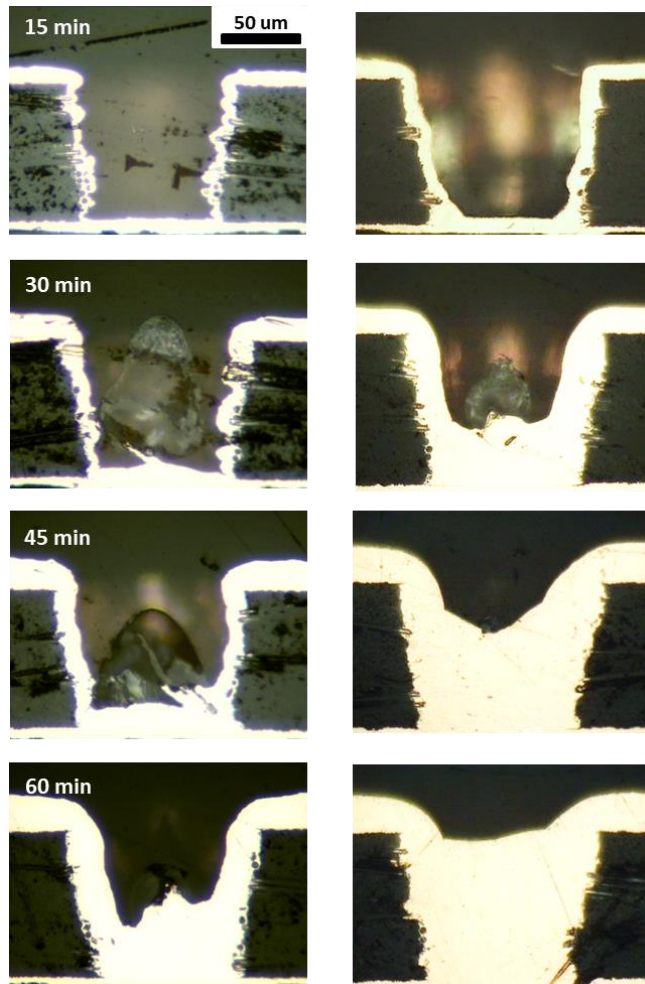
Figure 1. Cross-sectional images of copper electroplated in microvia without the synthesized leveler (left) and with the leveler (right).
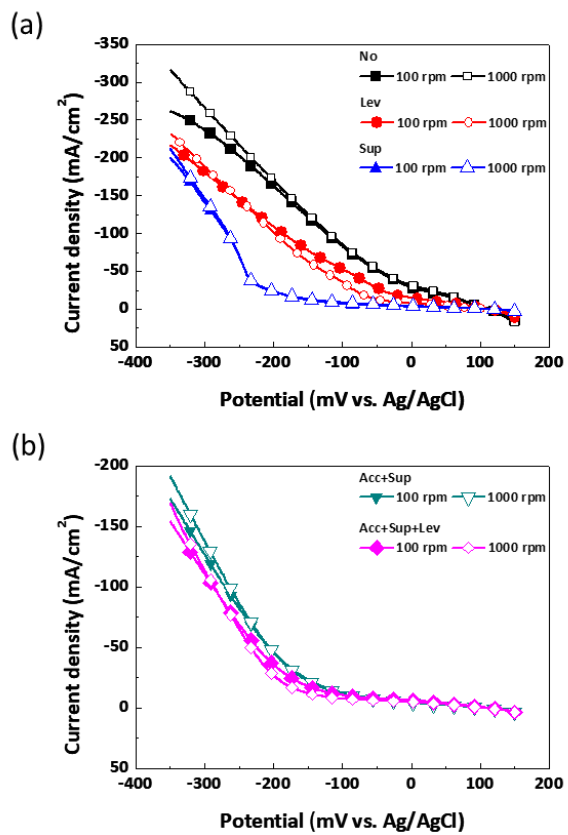
Figure 2. Linear sweep voltammograms for Cu electroplating on a Cu RDE (100 and 1000 rpm) with (a) the leveler (Lev) and suppressor (Sup) and (b) the accelerator (Acc)–Sup and Acc–Sup–Lev.
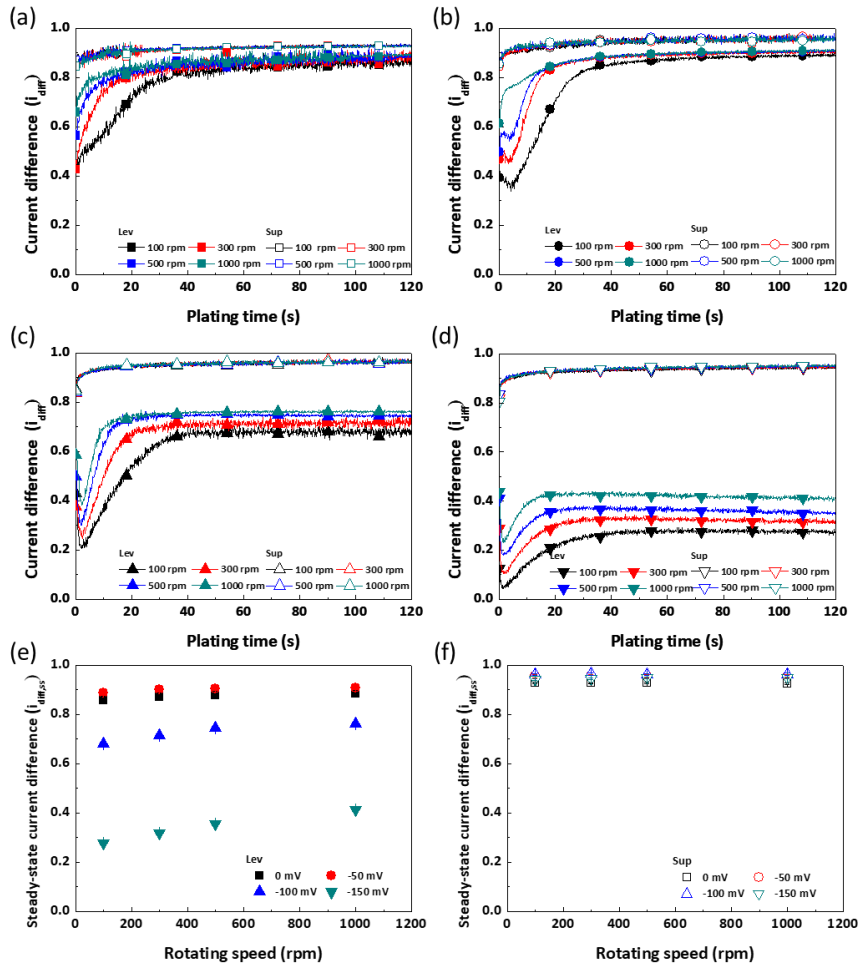
Figure 3. The plot of current difference (i_{diff}) for Cu electroplating with the leveler (Lev) and the suppressor (Sup) against the measurement time at applied potentials of (a) 0, (b) −50, (c) −100, and (d) −150 mV. The plot of steady-state current difference ($i_{\text{diff,ss}}$) for Cu electroplating with (e) Lev and (f) Sup against rotating speeds of 100, 300, 500, and 1000 rpm.
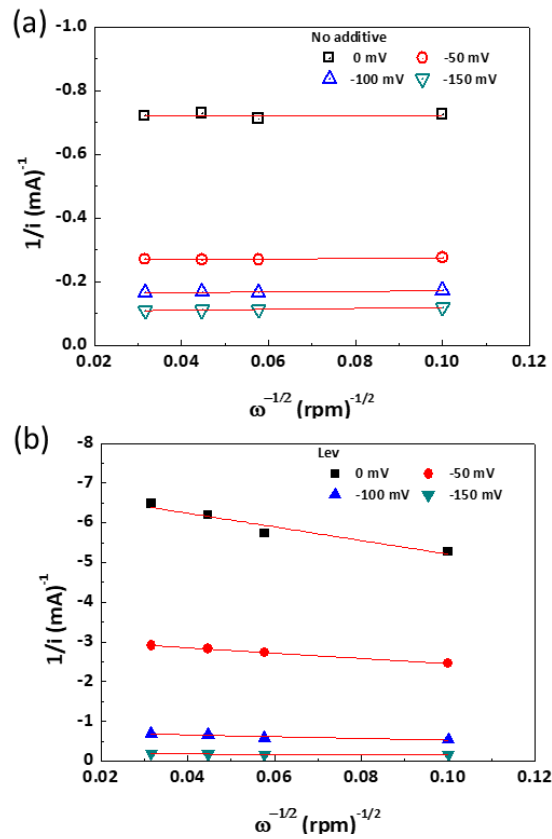
Figure 4. Koutecký–Levich plots for Cu electroplating (a) without and (b) with the leveler.

4. Conclusion

In this study, a quaternary ammonium-based leveler was synthesized and successfully adopted into Cu electroplating for microvia fill. In the LSV analysis, the leveler showed a convection-dependent inhibition, which would enable bottom-up filling. Its adsorption behavior was investigated with chronoamperometric measurements, and its convection-dependency was confirmed. The negative slope of the Koutecký–Levich plots for Cu electroplating with the leveler was also be related to the CDA of the leveler.

5. Reference

1. W.-P. Dow, M.-Y. Yen, W.-B. Lin, and S.-W. Ho, *J. Electrochem. Soc.*, **152**, C769–C775 (2005).

2. Takeshi Kobayashi, J. Kawasaki, K. Mihara, and H. Honma, *Electrochimica Acta*, **47**, 85–89 (2001).

3. S.-K. Kim, D. Josell, and T. P. Moffat, *J. Electrochem. Soc.*, **153**, C826–C833 (2006).

4. H.-C. Tsai, Y.-C. Chang, and P.-W. Wu, *Electrochem. Solid-State Lett.*, **13**, D7–D10 (2010).

5. M. Hayase, M. Taketani, K. Aizawa, T. Hatsuzawa, and K. Hayabusa, *Electrochem. Solid-State Lett.*, **5**, C98–C101 (2002).

6. W.-P. Dow and C.-W. Liu, *J. Electrochem. Soc.*, **153**, C190–C194 (2006).

7. P. Taephaisitphongse, Y. Cao, and A. C. West, *J. Electrochem. Soc.*, **148**, C492–C497 (2001).

8. W.-P. Dow, H.-S. Huang, and Z. Lin, *Electrochem. Solid-State Lett.*, **6**, C134–C136 (2003).

9. N. Xiao, N. Li, G. Cui, D. Tian, S. Yu, Q. Li, and G. Wu, J. Electrochem. Soc., **160**, D188–D195 (2013).

10. C. Wang, J. Zhang, P. Yang, and M. An, *Electrochimica Acta*, **92**, 356–364 (2013).

11. W.-P. Dow and C.-W. Liu, *J. Electrochem. Soc.*, **153**, C190–C194 (2006).

12. W.-P. Dow, C.-C. Li, M.-W. Lin, G.-W. Su, and C.-C. Huang, *J. Electrochem. Soc.*, **156**, D314–D320 (2009).

13. M. J. Kim, H. C. Kim, and J. J. Kim, *J. Electrochem. Soc.*, **163**, D434–D441 (2016).

14. J. J. Kelly, C. Tian, and A. C. West, *J. Electrochem. Soc.*, **146**, 2540–2545 (1999).

15. M. Takeuchi, Y. Yamada, M. Bunya, S. Okada, N. Okamoto, T. Saito, and K. Kondo, J. Electrochem. Soc., **160**, D3110–D3115 (2013).

16. M. Takeuchi, K. Kondo, H. Kuri, M. Bunya, N. Okamoto, and T. Saito, J. Electrochem. Soc., **159**, D230–D234 (2012).

17. A. Wang, B. Chen, L. Fang, J. Yu, and L. Wang, *Electrochimica Acta*, **108**, 698–706 (2013).

18. W. Wang, H. Hua, L. Yin, and Y. He, *J. Electrochem. Soc.*, **161**, D651–D656 (2014).

19. K. Kondo and R. N. Akolkar, in Copper Electrodeposition for Nanofabrication of Electronics Devices, p. 273, Springer, New York (2014)

20. Q. Zhang, X. Yu, Y. Hua, and W. Xue, *J. Appl. Electrochem.*, **45**, 79–86 (2015).

21. N. T. M. Hai, S. Furukawa, T. Vosch, S. D. Feyter, P. Broekmann, and K. Wandelt, Phys. Chem. Chem. Phys., **11**, 5422–5430 (2009).

22. J.-J. Sun, K. Kondo, T. Okamura, S. J. Oh, M. Tomisaka, H. Yonemura, M. Hoshino, and K. Takahashi, J. Electrochem. Soc., **150**, G355–G358 (2003).

23. K. Kondo, T. Yonezawa, D. Mikami, T. Okubo, Y. Taguchi, K. Takahashi, and D. P. Barkey, J. Electrochem. Soc., **152**, H173–H177 (2005).

24. M. J. Kim, Y. R. Seo, J. H. Oh, Y. J. Lee, H. C. Kim, Y. G. Kim, and J. J. Kim, J. Electrochem. Soc., **163**, D185–D187 (2016).

25. K. Kondo, Y. Yamada, and M. Yokoi, *J. Electrochem. Soc.*, **162**, D397–D400 (2015).

26. W.-P. Dow, H.-S. Huang, M.-Y. Yen, and H.-C. Huang, *J. Electrochem. Soc.*, **152**,

C425–C434 (2005).

27. W.-P. Dow, M.-Y. Yen, C.-W. Chou, C.-W. Liu, W.-H. Yang, and C.-H. Chen, Electrochem. Solid-State Lett., **9**, C134–C137 (2006).

28. V. Paneccasio, X. Lin, P. Figura, and R. Hurtubise, U.S. Pat., 7,309,992 (2007).

28. H. Qiu, L. Lv, B.-C. Pan, Q.-J. Zhang, W.-M. Zhang, and Q.-X. Zhang, J. Zhejiang Univ.-Sci. A, **10**, 716–724 (2009).

29. A. J. Bard and L. R. Faulkner, in Electrochemical Methods: Fundamentals and Applications, vol. 13, p. 568, Wiley, New York (2000).

31. H. Yang, A. Dianat, M. Bobeth, and G. Cuniberti, *J. Electrochem. Soc.*, **164**, D196–D203 (2017).

32. K. Kondo and R. N. Akolkar, in Copper Electrodeposition for Nanofabrication of Electronics Devices, p. 35, Springer, New York (2014)

Appendix II

Synthetic procedure of TEG-based levelers containing various terminal functional groups

* Yoonjae Lee in Laboratory of prof. Young Gyu Kim contributed to synthetic procedure.

TEG-based levelers containing various terminal functional groups were studied in Section 3.2.

1. General procedures

All the chemicals were obtained from commercial sources and were used without further purification. Tetrahydrofuran (THF) was distilled immediately prior to use from sodium and benzophenone under nitrogen atmosphere. Air or moisture sensitive reactions were carried out under nitrogen atmosphere using oven-dried glassware. The reactions were monitored with TLC silica gel 60 F_{254} plate, stained with a phosphomolybdic aicd or a ninhydrin stain solution. Column chromatography was performed on silica gel 60 (70-230 mesh). ^{1}H and ^{13}C nuclear magnetic resonance (NMR)

spectra were measured at 400 MHz and 100 MHz, respectively, in deuterated chloroform (CDCl₃) or deuterated methanol (MeOH-d_4) with Bruker Avance-400. The ^{1}H and ^{13}C NMR spectroscopic data were reported in ppm (δ) from the internal standard (TMS, 0.0 ppm) or residual solvent peaks of CDCl₃ (7.26 ppm and 77.16 ppm, respectively) or MeOH-d_4 (3.31 ppm and 49.00 pp m, respectively): chemical shift (integration, multiplicity, coupling constant in Hz). High resolution mass spectra (HRMS) were measured by the fast atom bombardment (FAB) ionization method and analyzed with a magnetic sector mass analyzer.

2. Synthesis of Lev 1, 2, 3, and 4

To a solution of 1,2″-bis(*N,N*-dimethylaminomethyl) triethylene glycol (**1**)[1] (367 mg, 1.39 mmol) in tetrahydrofuran (THF, 3 mL) and methanol (MeOH, 3 mL), allyl bromide (0.26 mL, 3.05 mmol, 2.2 equiv.) was added at room temperature. After 12 hrs, the reaction mixture was concentrated under the reduced pressure. The obtained crude mixture was diluted with H2O (20 mL) and washed with ethyl acetate (EtOAc, 20 mL) and the combined aqueous layer was concentrated under the reduced pressure to give a 1,2″-bis(*N,N,N*-dimethylallylaminomethyl) triethylene glycol dibromide (**Lev 1**) as

viscous yellowish liquid (581 mg, 83%); ^{1}H NMR (MeOH-d_4) δ 3.19 (12H, d, J=10),

3.41-3.60 (8H, m), 3.70 (4H, s), 4.11-4.16 (4H, m), 4.38 (2H, br s), 5.73-5.77 (4H, m),

6.10-6.18 (2H, m); ^{13}C NMR (MeOH-d_4) δ 50.6, 50.9, 64.7, 66.3, 67.6, 70.5, 73.0, 125.2,

128.2; HRMS for **Lev 1** (FAB) calcd for $C_{18}H_{38}BrN_2O_4^+$ 425.2015 ([M-Br]$^+$), found

425.2010; **Lev 3** and **Lev 4** were synthesized in the same procedure above by replacing

allyl bromide with benzyl bromide and 2-(bromomethyl) naphthalene, respectively. 1,2″-

bis(*N,N,N*-benzyldimethylaminomethyl) triethylene glycol dibromide (**Lev 3**) was

obtained as viscous yellowish liquid (3,661 mg, 94%); ^{1}H NMR (MeOH-d_4) δ 3.14 (6H,

s), 3.19 (6H, s), 3.45-3.62 (8H, m), 3.72 (4H, s), 4.47 (2H, br s), 4.69 (4H, ABq, J=12.8),

7.55-7.58 (6H, m), 7.63-7.65 (4H, m); ^{13}C NMR (MeOH-d_4) δ 50.1, 50.4, 64.8, 66.5,

69.0, 70.5, 73.1, 127.6, 128.9, 130.5, 133.1; HRMS for **Lev 3** (FAB) calcd for

$C_{26}H_{42}BrN_2O_4^+$ 525.2328 ([M-Br]$^+$), found 525.2317; 1,2″-bis(*N,N,N*-

dimethylnaphthylmethylaminomethyl) triethylene glycol dibromide (**Lev 4**) was

obtained as viscous yellowish liquid (14,803 mg, 82%); ^{1}H NMR (MeOH-d_4) δ 3.18 (6H,

s), 3.24 (6H, s), 3.51-3.62 (8H, m), 3.72 (4H, s), 4.48 (2H, br s), 4.84 (4H, ABq, J=13.2),

7.60-7.64 (4H, m), 7.67-7.70 (2H, m), 7.95-8.03 (6H, m), 8.19 (2H, s); ^{13}C NMR

(MeOH-d_4) δ 50.2, 50.5, 64.8, 66.5, 69.0, 70.5, 73.1, 124.9, 126.7, 127.4, 127.5, 128.2,

128.6, 129.1, 133.0, 133.7, 134.0; HRMS for **Lev 4** (FAB) calcd for $C_{34}H_{46}BrN_2O_4^+$

625.2641 ([M-Br]$^+$), found 625.2635; **Lev 2** was synthesized in the same procedure above except that the excess amount of propyl bromide (10 equiv.) was used in the neat conditions. 1,2″-bis(*N,N,N*-dimethypropylaminomethyl) triethylene glycol dibromide (**Lev 2**) was obtained as viscous yellowish liquid (1,796 mg, 64%). ^{1}H NMR (MeOH-d_4) δ 1.04 (6H, t, *J*=7.2), 1.81-1.90 (4H, m), 3.21 (12H, d, *J*=4.8), 3.40-3.60 (12H, m), 3.71 (4H, s), 4.33 (2H, br s); ^{13}C NMR (MeOH-d_4) δ 9.5, 15.8, 51.1, 51.4, 64.7, 66.3, 66.9, 70.5, 73.0; HRMS for **Lev 2** (FAB) calcd for $C_{18}H_{42}BrN_2O_4^+$ 429.2328 ([M-Br]$^+$), found 429.2327.

3. Reference

1. M. J. Kim, Y. R. Seo, J. H. Oh, Y. J. Lee, H. C. Kim, Y. G. Kim, and J. J. Kim, *J. Electrochem. Soc.*, **163**, D185–D187 (2016).

Appendix III

Synthetic procedure of TEG-based levelers according to the number of ammonium groups

* Yoonjae Lee in Laboratory of prof. Young Gyu Kim contributed to synthetic procedure.

TEG-based levelers according to the number of ammonium groups were studied in Section 3.3.

1. General procedures

All the chemicals were obtained from commercial sources and were used without further purification. Air or moisture sensitive reactions were carried out under nitrogen atmosphere using oven-dried glassware. The reactions were monitored with TLC silica gel 60 F_{254} plate, stained with a *p*-anisaldehyde or a ninhydrin stain solution. Column chromatography was performed on silica gel 60 (70-230 mesh). ^1H and ^{13}C nuclear magnetic resonance (NMR) spectra were measured at 400 MHz and 100 MHz, respectively, in deuterated chloroform ($CDCl_3$) or deuterated methanol (MeOH-d_4) with

Bruker Avance-400. The ^{1}H and ^{13}C NMR spectroscopic data were reported in ppm (δ) from the internal standard (TMS, 0.0 ppm) or residual solvent peaks of CDCl$_3$ (7.26 ppm and 77.16 ppm, respectively) or MeOH-d_4 (3.31 ppm and 49.00 pp m, respectively): chemical shift (integration, multiplicity, coupling constant in Hz). High resolution mass spectra (HRMS) were measured by the fast atom bombardment (FAB) ionization method and analyzed with a magnetic sector mass analyzer.

2. Synthesis of butanol oxiranylmethyl ether (2)

Sodium hydride (55% NaH, 1,310 mg, 30 mmol) was slowly added to a solution of butanol (1.84 mL, 20 mmol) dissolved in N,N-dimethylformamide (DMF, 8 mL) at 0 °C and stirred for 30 min under nitrogen atmosphere. Then, tetrabutylammonium iodide (Bu$_4$N$^+$I$^-$, 792 mg, 2 mmol) and allyl bromide (2.6 mL, 30 mmol) were added to a reaction mixture and stirred at room temperature for 7 hrs. The reaction mixture was quenched with addition of distilled water (2 mL), and the resulting mixture was partitioned between diethyl ether (Et$_2$O, 20 mL) and distilled water (10 mL). The separated organic layer was washed with distilled water (10 mL × 2), and the combined organic layers were dried over MgSO$_4$, filtered, and concentrated under the reduced

pressure. The obtained crude mixture of **1** and *meta*-chloroperoxybenzoic acid (75% *m*CPBA, 4757 mg, 20.7 mmol) was dissolved in dichloromethane (CH_2Cl_2, 40 mL) and the solution was refluxed for 6 hrs. Then, the reaction mixture was diluted with CH_2Cl_2 (20 mL) and washed with sat. $NaHCO_3$ (20 mL x 3). The organic layer was dried over $MgSO_4$, filtered, and concentrated under the reduced pressure. The crude mixture was purified by silica gel column chromatography with the gradient eluents (16:1 to 8:1 hexane:EtOAc) to afford compound **2** (1,348 mg, 52% in two steps) as colorless oil; ^{1}H NMR ($CDCl_3$) δ 2.60-2.62 (2H, dd, *J*=4.8, 2.8), 2.78-2.81 (2H, dd, *J*=4.8, 4), 3.15-3.18 (2H, m), 3.41-3.46 (2H, m), 3.65-3.71 (54H, m), 3.77-3.81 (2H, m); ^{13}C NMR ($CDCl_3$) δ 43.9, 50.5, 70.3, 70.5, 71.7; HRMS (FAB) calcd for $C_8H_{15}O_4^+$ 175.0970 ($[M+H]^+$), found 175.0974.

3. Synthesis of 2-(N,N-dimethylaminomethyl) ethylene glycol butanol ether (3)

N,N-Dimethylamine (2 M in MeOH, 6 mL, 12 mmol) was added to **2** (314 mg, 2.4 mmol) at room temperature. After 12 hrs, the reaction mixture was concentrated under reduced pressure to give 2-(N,N-dimethylaminomethyl) ethylene glycol butanol ether **3**

as yellowish oil (2.3 g, 96%); ^{1}H NMR δ 2.31 (2H, m), 2.33 (12H, s), 2.48 (2H, m), 3.49 (2H, m), 3.57 (2H, m), 3.70 (4H, s), 3.90 (2H, m); ^{13}C NMR δ 45.8, 61.9, 67.0, 70.9, 74.1; HRMS (FAB) calcd for $C_{12}H_{29}N_2O_4^+$ 265.2127 ([M+H]$^+$), found 265.2125.[3]

4. Synthesis of Lev A-1

Allyl bromide (0.38 mL, 4.4 mmol) was added to a solution of 2-(N,N-dimethylaminomethyl) ethylene glycol butanol ether (**3**) in methanol 10 mL and the resulting mixture was stirred for 12 hrs at room temperature. Then, the reaction mixture was concentrated under the reduced pressure. The obtained crude mixture was diluted with distilled water (10 mL), washed with EtOAc (10 mL x 2), and the combined aqueous layer was concentrated under the reduced pressure to give **Lev A-1** as viscous yellowish oil (1,057 mg, 3.6 mmol); ^{1}H NMR (CDCl$_3$) δ 0.94-0.98 (3H, t, J=7.2), 1.39-1.44 (2H, m), 1.55-1.61 (2H, m), 3.18-3.20 (6H, d, J=8.0), 3.38-3.46 (3H, m), 3.49-3.53 (3H, m), 4.07-4.17 (2H, m), 4.34-4.36 (1H, m), 5.72-5.76 (2H, m), 6.08-6.19 (1H, m); ^{13}C NMR (CDCl3) δ 44.4, 50.9, 70.7, 70.9, 72.1; HRMS (FAB) calcd for $C_{12}H_{29}N_2O_4^+$ 265.2127 ([M+H]$^+$), found 265.2125.[3]

5. Synthesis of glycerol triallyl ether (4)

Sodium hydride (55% NaH, 2,378 mg, 90 mmol) was slowly added to a solution of glycerol (1.46 mL, 20 mmol) dissolved in DMF (25 mL) at 0 °C and stirred for 30 min under nitrogen atmosphere. Then, tetrabutylammonium iodide (Bu$_4$N$^+$I$^-$, 3,928 mg, 6 mmol) and allyl bromide (7.8 mL, 90 mmol) were added to a reaction mixture and stirred at room temperature for 8 hrs. The reaction mixture was quenched with addition of distilled water (5 mL), and the resulting mixture was partitioned between Et$_2$O (40 mL) and distilled water (30 mL). The separated organic layer was washed with distilled water (20 mL × 2), and the combined organic layers were dried over MgSO$_4$, filtered, and concentrated under the reduced pressure. The crude mixture was purified by silica gel column chromatography with the gradient eluents (16:1 to 4:1 hexane:EtOAc) to afford compound **4** (2,871 mg, 68%) as colorless oil; ^{1}H NMR (CDCl$_3$) δ 3.59-3.68 (50H, m), 4.03 (4H, m), 5.17-5.30 (4H, m), 5.87-5.97 (2H, m); ^{13}C NMR (CDCl3) δ 44.4, 50.9, 70.7, 70.9, 72.1; HRMS (FAB) calcd for C$_{12}$H$_{29}$N$_2$O$_4$$^+$ 265.2127 ([M+H]$^+$), found 265.2125.

6. Synthesis of glycerol tris(oxiranylmethyl) ether (5)

A solution of compound **4** (978 mg, 4.61 mmol) and *meta*-chloroperoxybenzoic acid (75% *m*CPBA, 4,646 mg, 20.7 mmol) dissolved in dichloromethane (CH_2Cl_2, 35 mL) was refluxed for 8 hrs. Then, the reaction mixture was diluted with CH_2Cl_2 (30 mL) and washed with sat. $NaHCO_3$ (40 mL x 3). The organic layer was dried over $MgSO_4$, filtered, and concentrated under the reduced pressure. The crude mixture was purified by silica gel column chromatography with the gradient eluents (2:1 to 1:2 hexane:EtOAc) to afford compound **5** (721 mg, 60%) as colorless oil; ^1H NMR ($CDCl_3$) δ 2.62-2.65 (3H, m), 2.79-2.81 (3H, dd, J=4.8, 4.4), 3.14-3.18 (3H, m), 3.39-3.44 (2H, m), 3.55-3.67 (5H, m), 3.72-3.75 (1H, m); 3.78-3.82 (2H, m), 3.90-3.94 (1H, m); ^{13}C NMR ($CDCl_3$) δ 44.4, 50.9, 70.7, 70.9, 72.1; HRMS (FAB) calcd for $C_{12}H_{29}N_2O_4^+$ 265.2127 ($[M+H]^+$), found 265.2125.

7. Synthesis of glycerol tris[2-(N,N-dimethylaminomethyl)ethylene glycol] ether (6)

N,N-Dimethylamine (2 M in MeOH, 12 mL, 24 mmol) was added to **2** (721 mg, 2.8

mmol) at room temperature. After 12 hrs, the reaction mixture was concentrated under reduced pressure to give glycerol tris[2-(N,N-dimethylaminomethyl)ethylene glycol] ether **6** as yellowish oil (2.3 g, 96%); ^{1}H NMR (CDCl$_3$) δ 2.48-2.51 (18H, d, J=14.4), 2.62-2.71 (6H, m), 3.43-3.51 (4H, m), 3.54-3.66 (6H, m), 3.68-3.72 (1H, m), 3.92-3.98 (3H, m); ^{13}C NMR δ 45.8, 61.9, 67.0, 70.9, 74.1; HRMS (FAB) calcd for C$_{12}$H$_{29}$N$_2$O$_4^+$ 265.2127 ([M+H]$^+$), found 265.2125.

8. Synthesis of Lev A-3

Allyl bromide (0.82 mL, 9.5 mmol) was added to a solution of glycerol tris[2-(N,N-dimethylaminomethyl)ethylene glycol] ether (**6**) in methanol 15 mL and the resulting mixture was stirred for 12 hrs at room temperature. Then, the reaction mixture was concentrated under the reduced pressure. The obtained crude mixture was diluted with distilled water (10 mL), washed with EtOAc (10 mL x 2), and the combined aqueous layer was concentrated under the reduced pressure to give **Lev A-3** as viscous yellowish oil (2,069 mg, 2.7 mmol); ^{1}H NMR (CDCl$_3$) 3.20-3.23 (18H, d, J=10.0), 3.46-3.50 (6H, m), 3.52-3.60 (6H, m), 3.65-3.71 (4H, m), 3.80-3.83 (1H, m), 4.10-4.17 (6H, m), 4.41-4.42 (3H, m), 5.75-5.78 (6H, d, J=11.2), 6.10-6.21 (3H, m); ^{13}C NMR (CDCl3) δ 44.4,

50.9, 70.7, 70.9, 72.1; HRMS (FAB) calcd for $C_{12}H_{29}N_2O_4^+$ 265.2127 ([M+H]$^+$), found

265.2125.[3]